LA-UR-23-33566

Approved for public release; distribution is unlimited.

Title:	Statistical Analysis of the Limiting Dynamics of Two dimensional Boussinesq Turbulent Systems
Author(s):	Xie, Xuping
Intended for:	Report
Issued:	2023-12-05

Statistical Analysis of the Limiting Dynamics of Two dimensional Boussinesq Turbulent Systems*

Xuping Xie[1], Andrew J. Majda†[2], and Di Qi[3]

[1]Los Alamos National Laboratory
[2]Courant Institute, New York University
[3]Department of Mathematics, Purdue University

Abstract

In the current study, we investigate rotational and stratified turbulent systems within the framework of the Boussinesq equations. The effects of rotation and stratification give rise to a variety of dynamical regimes in atmospheric and oceanic turbulence. To develop a better understanding of the fundamental flow properties through a more straightforward mathematical framework, we commence our research with a simplified two-dimensional Boussinesq model that incorporates rotation and stratification effects. We explore two distinct limiting dynamics, considering pure rotation and pure stratification separately. We examine these intriguing dynamics through numerical investigations, applying the exact solution theory of Boussinesq equations and examining small-scale perturbations to the exact solution under rotation and stratification. We conduct an analysis of statistical quantities associated with the turbulent state variables. The results indicate that, under weak rotation at the equilibrium statistical state, the flow field exhibits vortex flow. However, strong rotation transforms the flow into vertical shear flow. We observe both downscale and upscale energy transfers with a decay rate of k^{-3} in the absence of external forcing and dissipation. Furthermore, we delve into the study of internal gravity wave mode interactions in the simplified two-dimensional Boussinesq system, which is a crucial aspect of geophysical turbulence due to gravity. Our findings reveal that the time series of the mode coefficients exhibit wave-like interactions between wave modes.

*This work was primarily conducted when the first author served as a Postdoc working with Prof. A.J.Majda at the Courant Institute.

†*In memory of Professor Andrew J. Majda, who passed away on March 12, 2021.*

Contents

1 Introduction

In this effort, we are studying rotational and stratified turbulent systems within the framework of Boussinesq equations. Rotation and stratification play essential roles in atmospheric and oceanic turbulence, leading to rich dynamical regimes. Quantifying and predicting such intriguing turbulent dynamics presents significant challenges. The two main objectives are statistical analysis and uncertainty quantification of these systems. The effects of rotation and stratification result in various dynamical regimes in atmospheric and oceanic turbulence. To gain a better understanding of the basic flow properties through a simpler mathematical setup, we initiate our investigation with a simplified two-dimensional Boussinesq model that accounts for rotation and stratification effects. The goals of this project are summarized as follows:

- We will begin by examining the two limiting dynamics of the 2D Boussinesq model with exact solutions. These two dynamic cases are as follows: i) strong stratification without rotation, and ii) strong rotation without stratification. It is essential to establish a clear understanding of how energy decays and transfers between different scales under these limiting dynamics.

- In addition to the elementary exact solutions within the limiting dynamics, we also aim to investigate the effects of small-scale perturbations on these exact solutions. For this purpose, we will employ direct numerical simulations to study the impact of perturbations in these simplified dynamic cases.

- In the case of rotational and stratified turbulent flows with high dimensions, developing a statistics-based reduced-order model for uncertainty quantification and the prediction of statistics in dominant leading directions is valuable. We will then apply the recent statistical closure model reduction strategy to these turbulent systems. [10].

There are many natural instances in atmosphere and ocean dynamics in which flows are driven by the rotation and stable density stratification. Rotation and stratification are most important features in the atmosphere and ocean dynamics. The classical Boussinesq approximation has a rich dynamical regime to study the effect of rotation and stratification in the atmosphere and ocean flows. In the certain range of scales, the fluid dynamics is controlled by the interaction of gravity and the earth's rotation with density variations about a background state. We introduce the full three dimensional Boussinesq equations with the following notation, $\vec{u} = (\vec{u}_H, w)$,

$$\frac{D^H}{Dt} = \frac{\partial}{\partial t} + \vec{u}_H \cdot \nabla_H, \quad \nabla_H = (\frac{\partial}{\partial x}, \frac{\partial}{\partial y}), \quad \mathrm{div}_H \vec{u}_H = \frac{\partial u}{\partial x} + \frac{\partial v}{\partial y}, \quad \vec{u}_H^{\perp} = (-v, u) \quad (1.1)$$

subscript H refer to the horizontal (x, y) directions. The three-dimension stratified ro-

tating viscous Boussinesq equations with forcing are the following,

$$\begin{aligned} \frac{D^H \vec{u}_H}{Dt} + w\frac{\partial \vec{u}_H}{\partial z} + f\vec{u}_H^{\perp} &= -\frac{1}{\rho_b}\nabla_H p \qquad &+\mu\Delta\vec{u}_H + \boldsymbol{F}_H, \\ \frac{D^H w}{Dt} + w\frac{\partial w}{\partial z} &= -\frac{1}{\rho_b}\frac{\partial p}{\partial z} - \frac{g}{\rho_b}\rho \qquad &+\mu\Delta w + \boldsymbol{F}_w, \\ \frac{D\rho}{Dt} + w\frac{\partial \overline{\rho}}{\partial z} &= \qquad &+\kappa\Delta\rho + \boldsymbol{F}_\rho, \\ div\ \vec{u} &= 0. \end{aligned} \tag{1.2}$$

Where the velocity field $\vec{u} = (u(x,y,z,t), v(x,y,z,t), w(x,y,z,t))$, μ is the viscosity of the fluid, f is the constant rotation frequency, κ is the thermal conductivity as a dissipation effect on ρ, and $\boldsymbol{F}_H, \boldsymbol{F}_w, \boldsymbol{F}_\rho$ represent forcing in the momentum and density equation. $\overline{\rho} = \rho_b - bz$ is the stratified mean density and $b > 0$ for stable stratification. The density field $\tilde{\rho}$ is decomposed into a reference constant ρ_b, background state $\overline{\rho}$, and fluctuations ρ,

$$\tilde{\rho} = \rho_b + \overline{\rho}(z) + \rho(\mathbf{x}, t).$$

The buoyancy frequency N in general is a function of z and defined by

$$N(z) = (-\frac{g}{\rho_b}\frac{d\overline{\rho}}{dz})^{\frac{1}{2}}, \tag{1.3}$$

with time independent $d\overline{\rho}/dz = -bz$ linearly dependents on z resulting in liner stratification. Stable stratification occurs when $b > 0$. In some case, the background density is a nonlinear function of z and time dependent, consequently, the buoyancy frequency becomes a time changing prameter. In order to identify different dynamical regimes, we introduce the following physical scales and numbers,

$$\vec{x}' = \frac{\vec{x}}{L},\ t' = \frac{t}{T_e},\ \vec{u}' = \frac{\vec{u}}{U},\ \rho' = \frac{\rho}{\rho_b B},\ p' = \frac{p}{\overline{p}} \tag{1.4}$$

$$Fr = \frac{U}{LN},\ \overline{P} = \frac{\overline{p}}{\rho_b U^2},\ \Gamma = \frac{BgL}{U^2},\ Ro = \frac{U}{Lf}. \tag{1.5}$$

We can write the nondimensional full Boussinesq equations without forcing as,

$$\begin{aligned} \frac{D^H \vec{u}_H}{Dt} + w\frac{\partial \vec{u}_H}{\partial z} &= -\overline{P}\nabla_H p - Ro^{-1}\vec{u}_H \qquad &+Re^{-1}\Delta\vec{u}_H, \\ \frac{D^H w}{Dt} + w\frac{\partial w}{\partial z} &= -\overline{P}p_z - \Gamma\rho \qquad &+Re^{-1}\Delta w, \\ \frac{D\rho}{Dt} &= \Gamma^{-1}Fr^{-2}w \qquad &+Re^{-1}Pr^{-1}\Delta\rho, \\ div\ \vec{u} &= 0. \end{aligned} \tag{1.6}$$

The Euler number $\overline{P}$ is the ratio of the pressure forces to inertial forces. The nondimensional number Γ is the ratio of the mean potential energy to the mean vertical kinetic

energy in the fluid. We make assumption that $\Gamma = Fr^{-1}$ to balance the buoyancy force in the vertical momentum equation ($Fr^{-1}\rho$) and the density changes from buoyant convection equation ($Fr^{-1}w$).

It is shown that the system (1.6) is controlled by the Froude number (Fr) and Rossby number (Ro) without dissipation and forcing. The Froude number can be considered as a measure of relative importance of buoyancy forces compared to the inertial forces (the ratio). In some atmosphere and ocean intermediate dynamical regime (mesoscales) where turbulence is generated in the presence of stable density stratification. The turbulence decaying is marked by the Froude number, $Fr = U/LN$. The turbulence starts when the inertial forces are dominating indicating a large Froude number. As the turbulence decays, the velocity U decreass and length scale L tends to grow, and the effects of stratification become important. When the buoyancy forces become of the order of the inertial foces, Froude number $Fr \sim 1$. As it decays further, the stratification dominates the flow with Froude number is very small $Fr << 1$. When effects of rotation are considered in the dynamics, such as large-scale flows in the atmosphere, the Rossby number Ro play an important role in changing the dynamics. The effects of the rotation is weak when Ro is large. For $Ro \sim 1$ in a highly stratified system ($Fr << 1$), the flow dynamics are significantly changed. It has been studied that under small Froude number and fixed Rossby number limiting case, the dynamics contain vertically sheared horizon motions [8]. As the Rossby number becomes small while the Froude number is small ($Ro = \epsilon Fr << 1$), the flow enters into the quasi-geostrophic state. The regime of stable stratification and weak rotation is of great importance in geophysical fluid dynamics since it describes fluid motions in the transition region between the small scales, energetic scales and the large scales at which energy is dissipated.

For the stably stratified Boussinesq systems, another important dynamical property is the internal gravity wave propagation. In the stratification, the fluid parcels oscillate owing to the restoring buoyancy force. The restoring buoyancy force acting on a vertically displaced fluid particle is characterized by the buoyancy frequency N defined in (1.3). In atmosphere and ocean flows, the scales of internal waves ranging from meters to kilometers. The wave period ranges from a fraction of an hour to a day. For longer time wave period, the effect of rotation induced by Coriolis force becomes important which modify the internal wave into inertia-gravity (IG) wave. Assume the solution has Fourier expansion $\exp(i\mathbf{k}\cdot\mathbf{x} + \omega t)$. Solving the eigenvalues of the linearized equations (1.2), the dispersion relation is given by,

$$\omega = 0, \;\; \omega^2 = \frac{N^2\mathbf{k}_H^2 + f^2 k_z^2}{\mathbf{k}^2}. \tag{1.7}$$

The above equation relates the wave frequency ω to the wave vector $\mathbf{k}$. The zero frequency $\omega = 0$ corresponds to purely horizontal motion. It is often referred as potential vortical mode. The nonzero solutions, $\pm\omega$, are the gravity wave mode. The mathematical quantity to distinction between wave and nonpropagating components is the Ertel's

potential vorticity,

$$q = (\vec{\omega} + f\vec{e}_3) \cdot \nabla\tilde{\rho}, \tag{1.8}$$

where $\vec{\omega} = \nabla \times \vec{u}$, and $\tilde{\rho}$ is the total density. In the absence of viscous and diffusive effects, Ertel's theorem [6] for the full Boussinesq system (1.2) without forcing tells us,

$$\frac{Dq}{Dt} = 0. \tag{1.9}$$

It indicates that q is conserved along fluid-parcel trajectories and does not contain wave propagation but advected by the flow. This property provides a decomposition in the flow dynamics, i.e., propagation wave and nonpropagation. The propagation wave part of the flow, corresponds to nonzero frequency ($\pm\omega$), does not contribute to the potential vorticity (PV). The nonpropagating component with zero frequency ($\omega = 0$), often called PV mode, accounts for all of the PV of the flow. In natural media, the internal gravity waves can be considered as short-time and short-scale perturbations. For this reason, the solution of the Boussinesq equations (1.6) can be decomposed into large scale motion and plane wave perturbations, often represented by slow dynamics and fast wave dynamics, respectively. In practical applications, e.g., weather forecasting, the fast gravity waves are filtered out and their effect upon the large scales are modeled through parameterizations [21, 22]. *Embid & Majda* developed a mathematically rigorous framework for deriving reduced slow dynamical equations for geophysical flows by averaging fast gravity waves, see [3, 4, 8, 9].

The interactions among the propagating waves and PV component are an important feature in the flows with internal gravity waves. The wave resonant theory was first introduced by Phillips (1960) [18, 19]. There are a lot of studies and theories have been introduced for the wave resonance, e.g., see [5, 14, 15, 17, 13, 20]. Three wave resonant interactions with phases $\mathbf{k} \cdot \mathbf{x} + \omega t$ occur if

$$\mathbf{k}_1 \pm \mathbf{k}_2 = \mathbf{k}_3, \text{and } \omega_1 \pm \omega_2 = \omega_3. \tag{1.10}$$

The three typical triad interactions are, *wave-wave-wave, wave-wave-PV, PV-PV-PV*. In the *wave-wave-wave* resonant triad, the interactions conserve energy since energy exchanges are confined to the wave field and there is no PV component. It can generate rapid growth of small scale disturbances, strong mixing as well as potential enstrophy which turn the flow into stratified turbulence. For *wave-wave-PV* resonance, there is no energy exchange between wave and PV component because of the conservation of potential vorticity. The PV mode acts as large scale slow dynamics whereas the two wave modes exchange energy inducing small scale fast dynamics, interested reader is refered to [3, 8]. The *PV-PV-PV* triad is presented in two-dimensional and quasi-geostrophic (QG) turbulence. The frequency condition is trivially satisfied for any three PV modes so that it causes strong inverse energy cascade and downscale enstrophy cascade. Another interaction, *wave-PV-PV*, is occurred in stratified, nonrotating (f=0) turbulence. This triad transfer PV mode energy to waves and then cascade to small dissipative

scales [1, 21].

The rotating stratified Boussinesq systems (1.2) provide a rich dynamical regime and different flow phenomena in atmosphere and ocean flow dynamics. It is challenging and important to understand those dynamics. In this work, we focus on a simplified two dimensional Boussinesq system in Section 2. We are interested in the two limiting dynamic cases with exact solution theory provided by *Majda* [6]. We will study how the two limiting dynamics react to the small scale perturbations in their exact solution. Numerical details will be discussed in Section 4.1. In this project, we study the rotational and stratified turbulent systems in the framework of Boussinesq equations. Rotation and stratification play an essential role in the atmosphere and oceanic turbulence, which lead to rich dynamical regimes. Quantifying and predicting such interesting turbulent dynamics are challenging. The two main objectives are statistical analysis and uncertainty quantification of such systems. The effects of rotation and stratification produce a variety of dynamical regimes for atmosphere and ocean turbulence. To gain a better understanding of the basic flow properties through a simpler mathematical setup, we start with a simplified two dimensional Boussinesq model with rotation and stratification effects. The goals of this work is to provide statistical analysis of the two limiting dynamics under the exact solution with small scale perturbation.

2 Two Dimensional Boussinesq dynamics

In this section, we present the simplified Boussinesq equations that will be extensively studied in this report. To simplify our initial study, we look at a simplified two dimensinoal Boussinesq system. Let the velocity field $\vec{u} = (u(x,z,t), v(x,z,t), w(x,z,t))$ has no dependence on y direction, i.e., $u_y = v_y = w_y = 0$. The full systems (1.2) become

$$\begin{aligned} u_t + uu_x + wu_z - fv &= -\frac{1}{\rho_b} p_x, \\ v_t + uv_x + wv_z + fu &= 0, \\ w_t + uw_x + ww_z &= -\frac{1}{\rho_b} p_z - \frac{g}{\rho_b}\rho, \\ \rho_t + u\rho_x + w\rho_z + w\frac{d\overline{\rho}}{dz} &= 0, \end{aligned} \tag{2.1}$$

This two dimensional equations offer a simpler formulation of the Boussinesq flow but still with direct link to the full three dimensional system. It becomes easier to first develop a better understanding of the flow dynamics based on the simpler formulation. Following the same scaling process in (1.4) and nondimensional numbers (1.5), we can have the nondimensional form of the simplified the two dimensional Boussinesq equations without

dissipation and forcing,

$$\begin{aligned}\frac{\partial \vec{u}_H}{\partial t} + \vec{u}\cdot\nabla\vec{u}_H &= -\overline{p}\nabla_H p - Ro^{-1}\vec{u}_H^{\perp},\\ \frac{\partial w}{\partial t} + \vec{u}\cdot\nabla w &= -\overline{p}p_z - Fr^{-1}\rho,\\ \frac{\partial \rho}{\partial t} + \vec{u}\cdot\nabla\rho &= Fr^{-1}w,\\ \nabla\cdot\vec{u} &= 0.\end{aligned} \tag{2.2}$$

Here, we have used the assumption $\Gamma = Fr^{-1}$ to balance the interaction effects between density ρ and vertical momentum w equations in (2.2). Both singular terms have the same coefficient Fr^{-1} and the combined contribution in the energy identity will cancel out. The Ertel's potential vorticity (PV) of system (2.1) is $q = \vec{\omega}_a\cdot\nabla\tilde{\rho}$ with the absolute vorticity $\vec{\omega}_a = \vec{\omega} + f\vec{e}_3 = (-v_z, \omega, v_x + f)^T$. In the nondimensional form, the potential voritiy of (2.2) has

$$q = v_x - \frac{Fr}{Ro}\rho_z - Fr(v_z\rho_x + v_x\rho_z), \tag{2.3}$$

with conservation property $Dq/Dt = 0$. We introduce a new nondimensional number

$$F = \frac{Fr}{Ro} = \frac{f}{N}, \tag{2.4}$$

be the ratio of rotation frequency f to buoyancy frequency N. It turns out that the equations (2.2) can be further simplified into the vorticity-stream formula to remove the pressure term in the equation,

$$\begin{aligned}\omega_t + \nabla^{\perp}\psi\cdot\nabla\omega &= Ro^{-1}v_z + Fr^{-1}\rho_x,\\ v_t + \nabla^{\perp}\psi\cdot\nabla v &= -Ro^{-1}u,\\ \rho_t + \nabla^{\perp}\psi\cdot\nabla\rho &= Fr^{-1}w,\\ \omega &= -\Delta\psi.\end{aligned} \tag{2.5}$$

with $(u, w)^T = (-\psi_z, \psi_x)^T$, $\omega = u_z - w_x$. Let $\boldsymbol{u} = (\omega, v, \rho)^T$, under the fourier space, the solution has the form $\boldsymbol{u} = \hat{\boldsymbol{u}}\exp(i\mathbf{k}\cdot\mathbf{x} - \sigma t)$, $\mathbf{k} = (k_x, k_z)$. Note that we use σ to denote the wave frequency in this simplified system to distinguish the vorticity ω, whereas the full three dimensional systems use ω for the frequency. The eigenvalue for the linear operator L reduces to the equation,

$$(-i\sigma I + L(i\mathbf{k}))\hat{\boldsymbol{u}} = 0, \tag{2.6}$$

with the matrix of given by,

$$L(i\mathbf{k}) = \begin{pmatrix} 0 & ik_z & F^{-1}ik_x\\ -ik_z/\mathbf{k}^2 & 0 & 0\\ F^{-1}ik_x/\mathbf{k}^2 & 0 & 0\end{pmatrix}. \tag{2.7}$$

The linear and nonlinear operators are given by

$$L\boldsymbol{u} = \begin{pmatrix} Fv_z + \rho_x \\ -Fu \\ w \end{pmatrix}, \quad B(\boldsymbol{u}, \boldsymbol{u}) = \begin{pmatrix} \nabla^{\perp}\psi \cdot \nabla\omega \\ \nabla^{\perp}\psi \cdot \nabla v \\ \nabla^{\perp}\psi \cdot \nabla\rho \end{pmatrix}. \tag{2.8}$$

The eigenvalues of the simplified two dimensional Boussinesq equations (2.1) determined from,

$$\sigma = 0, \;\; \sigma^2 = \frac{F^{-2}k_x^2 + k_z^2}{\mathbf{k}^2}, \tag{2.9}$$

which are very similar to the full three dimensional Boussinesq system (1.7). One thing to notice that $F = \frac{f}{N} = 1$ indicates the two dimensional dynamics is isotropic in the $xz-$ plane with liner dispersion relation $\sigma^2 = N^2$ (nondimensional form $\sigma^2 = 1$). The nonzero eigenvalues $\pm\sigma$ correspond to gravity waves and the zero eigenvalue correspond to vortical mode. The corresponding eigenfunctions are,

$$\boldsymbol{r}^0 = \begin{pmatrix} 0 \\ k_x \\ -Fk_z \end{pmatrix} \text{ vortical mode}, \;\; \boldsymbol{r}^{\pm} = \begin{pmatrix} \pm\mathbf{k}^2\sigma \\ -k_z \\ F^{-1}k_x \end{pmatrix} \text{ wave mode}. \tag{2.10}$$

This enables us to project the Fourier expansion of the solution to (2.5) onto the eigenfunction space, with the form

$$\boldsymbol{u} = a_0\boldsymbol{r}^0 + a_+\boldsymbol{r}^+ + a_-\boldsymbol{r}^- \tag{2.11}$$

The vortical mode with zero eigenvalue does not involve wave propagating. This interaction causes two dimensional turbulence with inverse energy cascade and downscale enstrophy cascade. In the Boussinesq framework, the PV component (no wave interaction) gives the quasi-geostrophic solution,

$$\boldsymbol{u} = a_0\boldsymbol{r}^0, \quad \text{geostrophic mode}, \tag{2.12}$$

with each velocity component satisfies

$$u = w = \omega = 0, \quad v = p_x, \quad \rho = -Fp_z, \;\; \text{and } p_{xx} + F^2p_{zz} = q, \tag{2.13}$$

where p is the pressure and the potential vorticity q is defined in (2.3). We will discover how the initial data in geostrophic balance evolve in the rotation and stratification limiting dynamics of the two dimensional Boussinesq. The total energy of (2.2) can be written as

$$E = \int \frac{1}{2}\vec{u}\cdot\vec{u} + \frac{1}{2}\rho^2 d\mathbf{x}, \tag{2.14}$$

with the first part considered as kinetic energy (KE) and latter referred to potential energy (PE). In the absence of dissipation and forceing, the total energy is conserved

$$\frac{dE}{dt} = \int \vec{u}\frac{d\vec{u}}{dt} + \rho\frac{d\rho}{dt} = \int \nabla\cdot(\vec{u}p), \tag{2.15}$$

as the integration taken under the periodic boundary condition. We can introduce generalized rotating stratified enstrophy of the two dimensional system (2.5) as the following

$$\mathcal{Z} = \frac{1}{2}\int \omega^2 + |\nabla v|^2 + |\nabla \rho|^2. \tag{2.16}$$

Its corresponding evolution equation

$$\frac{d\mathcal{Z}}{dt} = \int \nabla^{\perp} v \nabla \vec{u} \nabla^{\perp} v + \nabla^{\perp} \rho \nabla \vec{u} \nabla^{\perp} \rho, \tag{2.17}$$

show that the dynamics of $\mathcal{Z}$ is controlled by the strain flow which is similar to three dimensional turbulence. The pair of total energy E and enstrophy resemble the similar quantity of the full three dimensional turbulent systems. We can claim that the simplified two dimensional Boussinesq system (2.2) tends to generate small scales and a downscale energy cascade is expected. We shall exam the energy transfer mechanism between under different dynamics in our the numerical experiments.

2.1 Exact Solution

We want to ask that, given the elementary exact solution of the Boussinesq equations, how does the small scale perturbations change the dynamics and cause instability with rotation? In this section, we apply the exact solution theory to investigate the perturbations on the exact solution. This provides a more detailed characterization for the interactions between the large-scale structures and the fluctuation modes. In atmosphere and ocean where stably stratification occurs, the instability is very important to stratified turbulence. For stratified flow, the instability has a significant effect on large scale motion of the flow dynamics especially when rotation is considered, although mixing and turbulence are often suppressed in the flow. In this section, our goal is to study how the two dimensional Boussinesq system (2.5) react to the perturbations of the large scale flow under rotation in stably stratification. In [11, 12], *Majda & Shefter* studied the instability of elementary nonlinear solutions of Boussinesq equations without rotation at large Richardson number. Their results shown that, for stable stratification, there is transient large amplitude behavior yields instability at certain range of Richardson number and the initial perturbation can amplify with exponential growth in the beginning. We start with the steady time-independent shear flow [12] as the elementary exact solution of the two dimensional Boussinesq equations (2.5), and investigate the dynamics with different rotation scale controlled by the nondimensional number F defined in (2.4).

In the exact solution theory, the linear background density $\overline{\rho}$ is removed and the flow field can be decomposed into large scale and nonlinear plane wave perturbations,

$$\vec{u} = \mathcal{D}\mathbf{x} + \frac{1}{2}\vec{\omega}(t) \times \mathbf{x} + A(t)F(\alpha(t) \cdot \mathbf{x}), \tag{2.18}$$

$$\rho = \rho_b + \vec{b} \cdot \mathbf{x} + B(t)F(\alpha(t) \cdot \mathbf{x}). \tag{2.19}$$

Here, we do not consider the nonlinear plane wave exact solutions, more details can be found in *A.J. Majda's book* [6]. The $\vec{\omega}$ and $\vec{b}$ satisfy the following equations,

$$\frac{d\vec{\omega}}{dt} = \mathcal{D}(t)\vec{\omega} + \mathcal{D}(t)f\vec{e}_3 + \frac{1}{2}\begin{pmatrix} f\omega_2 \\ -f\omega_1 \\ 0 \end{pmatrix}, \tag{2.20}$$

$$\frac{d\vec{b}}{dt} = -\mathcal{D}(t)\vec{b} + \frac{1}{2}\vec{\omega} \times \vec{b}. \tag{2.21}$$

In other words, the linear density background profile $\overline{\rho}$ is replaced by the exact solution $\vec{b} \cdot \mathbf{x}$. We would like to study how the large scale exact solution $\vec{b} \cdot \mathbf{x}$ evolve with initial perturbations in different rotation force. We consider the following two sets of exact solution as the initial balanced data for our numerical experiments of (2.27).

Shear Flow It can be shown that the following shear flow satisfies the above exact solution scheme (2.20).

$$\begin{aligned} \vec{V} &= (A_1 Z + fy, A_2 Z - fx, 0)^T, \\ \vec{\Omega} &= (-A_2, A_1, -2f)^T, \\ \vec{b} &= (0, 0, -B_0)^T \\ \mathcal{D} &= \frac{1}{2}\begin{pmatrix} 0 & 0 & A_1 \\ 0 & 0 & A_2 \\ A_1 & A_2 & 0 \end{pmatrix} \end{aligned}$$

This shear flow is time independent without interaction of stretching and vorticity. It has flow pointing in one direction but depending in magnitude on another direction. For stably stratified flow, Miles-Howard theorem [16] states that steady shear flows $\vec{u} = (v(z), 0, 0)^T$ are linearly stable for all Richardson numbers. In [11], Majda studied the instability of time-dependent exact solutions of such flow at large Richardson number. Given this shear flow as the initial data, we would like to study

Geostrophic Balance It has been studied that, the stably stratified Boussinesq flow in the high stratification limit ($Fr << 1$) converged to two dimensional layered equations without dynamical interations among layers, see [9]. Furthermore, the effects of high rotation and high stratification turn the rotating Boussinesq equations (2.27) into quasi-geostrophic (QG) equations with asymptotic limit of small Rossby ($Ro << 1$) and Froude ($Fr << 1$) numbers, the details of rigorous mathematical proof can be found in [4, 6, 8]. The key feature of the QG limiting dynamics of Boussinesq equations is the balance between rotation and pressure force. In the two dimensional Boussinesq equations (2.27) with the previous nondimensional scaling, the geostrophic balance equations are given

by,

$$v = p_x, \qquad \text{geostrophic balance} \tag{2.22}$$

$$p_z = -F^{-1}\rho, \qquad \text{hydrostatic balance} \tag{2.23}$$

$$w = 0, \qquad \text{zero vertical velocity} \tag{2.24}$$

$$p_{xx} + F^2 p_{zz} = q, \qquad \text{conservation of PV} \tag{2.25}$$

where p is the pressure and q is the potential vorticity (2.3).

2.2 Two limiting dynamics

The rotation and stratification are two major effects for the Boussinesq system, which generate a wide range of interesting dynamics. Here, we start with two limiting cases where purely rotation or purely stratification are considered separately. Considering the nondimensional Rossy number $Ro = \frac{U}{Lf}$, the system (2.5) without constant liner density background becomes

$$\begin{aligned} \omega_t + \nabla^\perp\psi \cdot \nabla\omega &= Ro^{-1}v_z + \rho_x, \\ v_t + \nabla^\perp\psi \cdot \nabla v &= -Ro^{-1}u, \\ \rho_t + \nabla^\perp\psi \cdot \nabla\rho &= 0, \\ \omega &= -\Delta\psi. \end{aligned} \tag{2.26}$$

This limiting system only involve rotation effect, which can greatly help us understand how the system react to the small perturbation with exact solution theory. Another limiting case is purely stratification dynamics, given by the following equations,

$$\begin{aligned} \omega_t + \nabla^\perp\psi \cdot \nabla\omega &= Fr^{-1}\rho_x, \\ v_t + \nabla^\perp\psi \cdot \nabla v &= 0, \\ \rho_t + \nabla^\perp\psi \cdot \nabla\rho &= Fr^{-1}w, \\ \omega &= -\Delta\psi. \end{aligned} \tag{2.27}$$

As is known that, small Fr number indicates strong stratification whereas the large Froud number has weak stratification effect. It is similar to rotation force. These two limiting dynamical systems provide an easy way to analyze the effect of rotation and stratification separately controlled by the nondimensional Froud number and Rossby number. We will discover the energy transfer mechanism and statistical analysis for the two dynamics in our numerical section.

2.3 Wave-mode Interaction

As stated in the equation (2.11), the solution can be expanded by the three eigenmodes. Thus, it is interested to study how the three mode interact with each other. Here, we follow the same framework and project all the Fourier coefficients to the three eigenfunctions to obtain mode coefficients. Note that the eigenfunctions in (2.10) are not orthogonal. In order to obtain an orthonormal basis, we project and recover the eigenmodes to the

full velocity space by using $(\hat{u}, \hat{w}) = (-ik_z, ik_x)\hat{\psi}$ and $\hat{\psi} = \mathbf{k}^{-2}\hat{\omega}$. The orthonormal basis are hence given by,

$$\boldsymbol{r}^0 = \begin{pmatrix} 0 \\ ik_x \\ 0 \\ -Fik_z \end{pmatrix}, \quad \boldsymbol{r}^+ = \frac{1}{\sqrt{2}\sigma|\mathbf{k}|}\begin{pmatrix} -ik_z\sigma \\ Fk_z \\ ik_x\sigma \\ k_x \end{pmatrix}, \quad \boldsymbol{r}^- = \frac{1}{\sqrt{2}\sigma|\mathbf{k}|}\begin{pmatrix} ik_z\sigma \\ Fk_z \\ -ik_x\sigma \\ k_x \end{pmatrix}. \tag{2.28}$$

The Fourier coefficients of the full velocity space is given by,

$$\hat{\boldsymbol{u}}(\mathbf{k}, t) = a_0(\mathbf{k}, t)\boldsymbol{r}^0 + a_+(\mathbf{k}, t)\boldsymbol{r}^+ + a_-(\mathbf{k}, t)\boldsymbol{r}^-, \tag{2.29}$$

where $\hat{\boldsymbol{u}} = (\hat{u}, \hat{v}, \hat{w}, \hat{\rho})$, a_0, a_+, a_- are the mode coefficients which can be computed through the following projection,

$$a_\alpha(\mathbf{k}, t) = \hat{\boldsymbol{u}} \cdot \overline{\boldsymbol{r}^\alpha}, \tag{2.30}$$

as $\boldsymbol{r}^\alpha \cdot \overline{\boldsymbol{r}^\beta} = \delta_{\alpha\beta}$, $\delta_{\alpha\beta} = 1$, if $\alpha = \beta$, and 0 otherwise. In this study, we project all the Fourier coefficients to obtain the mode coefficients of system (2.27) and (4.10), and discuss the evolution of the coefficients and their interaction. The dynamic equation of the coefficients for three modes can be found in the form,

$$\frac{da_\alpha}{dt} + \sum_{k_x+k_z=|k|} \sum_{u,v} C_{uv}^\alpha(k_x, k_z)a_u(k_x)a_v(k_z) = 0 \tag{2.31}$$

3 Statistical Equations and Reduced-order Modeling

In this section, we outline the general equilibrium statistical mechanics for the Boussinesq turbulent systems. The turbulent dynamics are highly chaotic and unpredictable for single trajectory. However, there exists coherent patterns out of large ensembles of trajectories. We will discuss some quantities based on one-point statistics. Let $p(\boldsymbol{X})$ denotes the probability density measuring the turbulent state $\boldsymbol{u}$ with $\int p(\boldsymbol{X})d\boldsymbol{X} = 1$. The Gaussian densities are the most universal distributions with given first and second moment,

$$\overline{\boldsymbol{u}} = \int \boldsymbol{u}p(\boldsymbol{X})d\boldsymbol{X}, \quad \sigma^2 = \int (\boldsymbol{u} - \overline{\boldsymbol{u}})^2 p(\boldsymbol{X})d\boldsymbol{X}$$

The non-Gaussian features are contained in the third and fourth moments of a probability distribution. The third and fourth moments are characterized by the skewness and kurtosis,

$$Skew = \frac{\int (\boldsymbol{u} - \overline{\boldsymbol{u}})^3 p(\boldsymbol{X})d\boldsymbol{X}}{(\int (\boldsymbol{u} - \overline{\boldsymbol{u}})^2 p(\boldsymbol{X})d\boldsymbol{X})^{3/2}}, \quad Kurt = \frac{\int (\boldsymbol{u} - \overline{\boldsymbol{u}})^4 p(\boldsymbol{X})d\boldsymbol{X}}{(\int (\boldsymbol{u} - \overline{\boldsymbol{u}})^2 p(\boldsymbol{X})d\boldsymbol{X})^2}$$

From Ergodicity theory with proper assumption of the system, the statistical expectation can be calculated by averaging the time series in steady state,

$$\langle \boldsymbol{u} \rangle = \int p(\boldsymbol{X})\boldsymbol{u}d\boldsymbol{X} = \lim_{T\to\infty} \frac{1}{T} \int_{t_0}^{t_0+T} \boldsymbol{u}dt. \tag{3.1}$$

The general formulation of dynamical system (2.5) as,

$$\frac{\partial \boldsymbol{u}}{\partial t} = (L + D)\boldsymbol{u} + B(\boldsymbol{u}, \boldsymbol{u}) + \boldsymbol{F}(t) + \sigma \dot{\boldsymbol{W}}(t), \tag{3.2}$$

where the first operator L represents linear dispersion and satisfy skew-symmetry $L^* = -L$. The D operator represents dissipation effects in the system with property $D^* = D < 0$ ('*' means conjugate transpose of the matrix). The external forcing effects are decomposed into a deterministic component, $\boldsymbol{F}(t)$ and a stochastic component usually represented by a Gaussian random process, $\sigma(t)\dot{\boldsymbol{W}}(t)$. The nonlinear term in the dynamical system is represented by a general quadratic form, $B(\boldsymbol{u}, \boldsymbol{u})$, about the state variables $\boldsymbol{u}$ that conserves energy when linear operators and forcing are ignored, such that,

$$\boldsymbol{u} \cdot B(\boldsymbol{u}, \boldsymbol{u}) = \sum_{j=1}^{N} u_j B_j(\boldsymbol{u}, \boldsymbol{u}) = 0 \tag{3.3}$$

In the two dimensional Boussinesq system, the nonlinear effects are given by $B(\boldsymbol{u}, \boldsymbol{u}) = \nabla^{\perp}\psi \cdot \nabla \boldsymbol{u}$. We use a finite-dimensional fourier space, $\{\boldsymbol{\varphi}_i\}_{i=1}^N$, to represent the above dynamical system. The full turbulent state $\boldsymbol{u}$ can be decomposed into mean-fluctuation component.

$$\boldsymbol{u} = \langle \boldsymbol{u} \rangle + \boldsymbol{u}' = \overline{\boldsymbol{u}} + \sum_{i=1}^{N} \hat{\boldsymbol{u}}_i(t)\boldsymbol{\varphi}_i, \tag{3.4}$$

where $\overline{\boldsymbol{u}} = \langle \boldsymbol{u}(t) \rangle$ represents the ensemble average of the system solution, and $\hat{Z}_i(t)$ are stochastic coefficients measuring the fluctuation processes along the direction $\boldsymbol{\varphi}_i$. By using the mean-fluctuation decomposition, we can get the evolution equation of mean state $\overline{\boldsymbol{u}}$,

$$\frac{d\overline{\boldsymbol{u}}}{dt} = (L+D)\overline{\boldsymbol{u}} + B(\overline{\boldsymbol{u}}, \overline{\boldsymbol{u}}) + \sum_{i,j} R_{ij} B(\boldsymbol{\varphi}_i, \boldsymbol{\varphi}_j), \tag{3.5}$$

with $R = \langle \hat{\boldsymbol{Z}} \hat{\boldsymbol{Z}}^* \rangle$ the second order covariance matrix of the fluctuation coefficients $\{\hat{Z}_i\}_{i=1}^N$. The term $B(\overline{\boldsymbol{u}}, \overline{\boldsymbol{u}})$ represents the nonlinear interaction of the mean state, and $R_{ij} B(\boldsymbol{\varphi}_i, \boldsymbol{\varphi}_j)$ is the higher-order feedbacks from the fluctuation modes to the mean state dynamics. The random fluctuation component of the solution, $\boldsymbol{u}' = \sum_{i=1}^N \hat{Z}_i(t) \boldsymbol{\varphi}_i$ satisfies

$$\frac{d\boldsymbol{u}'}{dt} = (L+D)\boldsymbol{u}' + B(\overline{\boldsymbol{u}}, \boldsymbol{u}') + B(\boldsymbol{u}', \overline{\boldsymbol{u}}) + B(\boldsymbol{u}', \boldsymbol{u}') - \langle B(\boldsymbol{u}', \boldsymbol{u}') \rangle + \sigma \dot{\boldsymbol{W}}(t), \tag{3.6}$$

Project the above fluctuation dynamics onto the orthonormal basis, we obtain

$$\frac{dZ_i}{dt} = Z_j[(L+D)\boldsymbol{\varphi}_j + B(\overline{\boldsymbol{u}}, \boldsymbol{\varphi}_j) + B(\boldsymbol{\varphi}_j, \overline{\boldsymbol{u}})] \cdot \boldsymbol{\varphi}_i + [B(\boldsymbol{u}', \boldsymbol{u}') - \langle B(\boldsymbol{u}', \boldsymbol{u}') \rangle] \cdot \boldsymbol{\varphi}_i + \sigma \dot{\boldsymbol{W}}(t) \cdot \boldsymbol{\varphi}_i, \tag{3.7}$$

Consequently, the exact evolution equation of the covariance matrix $R = \langle \hat{\boldsymbol{Z}} \hat{\boldsymbol{Z}}^* \rangle$ can be derived by multiplying Z_j^* on both sides of the above equation and taking ensemble statistical average

$$\frac{dR}{dt} = L_v(\overline{\boldsymbol{u}})R + RL_v^*(\overline{\boldsymbol{u}}) + Q_F + Q_\sigma, \tag{3.8}$$

where we have: 1) the linear dynamical operator $L_v(\overline{\boldsymbol{u}})$ expresses energy transfers between the mean field and the stochastic modes (effect due to B), as well as energy dissipation (effect due to D) and non-normal dynamics (effect due to L)

$$\{L_v\}_{ij} = [L+D]\boldsymbol{\varphi}_j + B(\overline{\boldsymbol{u}}, \boldsymbol{\varphi}_j) + B(\boldsymbol{\varphi}_j, \overline{\boldsymbol{u}}) \cdot \boldsymbol{\varphi}_i; \tag{3.9}$$

2) the positive definite operator Q_σ express energy transfer due to the external stochastic forcing

$$\{Q_\sigma\}_{ij} = \sum_k (\boldsymbol{\varphi}_i \cdot \sigma_k)(\sigma_k \cdot \boldsymbol{\varphi}_j); \tag{3.10}$$

3) as well as. the energy flux Q_F expresses nonlinear energy transfer between different modes due to non-Gaussian statistics modeled through third-order moments

$$\{Q_F\}_{ij} = \sum_{m,n} \langle Z_m Z_n Z_j \rangle B(\boldsymbol{\varphi}_m, \boldsymbol{\varphi}_n) \cdot \boldsymbol{\varphi}_i + \langle Z_m Z_n Z_i \rangle B(\boldsymbol{\varphi}_m, \boldsymbol{\varphi}_n) \cdot \boldsymbol{\varphi}_j. \tag{3.11}$$

Note that the energy conservation property of the quadratic operator B is inherited in the statistical equations by the matrix Q_F since

$$tr(Q_F) = 2 \sum_i \sum_{m,n} \langle Z_m Z_n Z_i \rangle B(\boldsymbol{\varphi}_m, \boldsymbol{\varphi}_n) \cdot \boldsymbol{\varphi}_i = 2B(\boldsymbol{u}', \boldsymbol{u}') \cdot \boldsymbol{u}' = 0. \tag{3.12}$$

The above exact statistical equations for the state of the mean and covariance matrix will be the starting point in development of reduced order model for two dimensional-Boussinesq turbulent systems. Note that the statistical dynamics for the mean (3.6) and covariance (3.8) are still not closed due to the inclusion of third order moments through the nonlinear interactions in Q_F in (3.11). The fundamental strategy for developing reduced-order model concerns the proper approximation about the energy flux term Q_F in a simple and efficient manner so that the energy mechanism can be modeled properly in the reduced surrogate model.

4 Numerical Experiments

4.1 Free-Decay

In this section, we present the numerical simulation results of the free-decay system (2.27) without stratification ($N = 0$) using shear flow as the initial data. We investigate the effect of small scale perturbations to the shear flow solution and the energy transfer behavior under different rotation forces. The simulations use Fourier pseudo-spectral method with $2/3$ dealiasing in space and the physical domain is $[x, z] \in [0, 2\pi] \times [0, 2\pi]$ with 128×128 Fourier mode. A sixth-order explicit Runge-Kutta scheme is used for time integration. We take the following non-dimensional scale for the shear flow solution:

$$Fr = \frac{U}{LN} = \frac{\omega_0}{N}, \;\; N^2 = \frac{gB_0}{\rho_b}(B_0 > 0), \;\; b = B_0 b',$$

Then the velocity becomes,

$$\vec{V} = (FrZ, -FX, 0)^T, \; \Omega = (0, \omega_0, -2F)^T, \; b = (0, 0, -1)^T \tag{4.1}$$

We use the shear flow solution and perturbations as the initial solution of (2.27),

$$\omega = \omega_0 + \sum_{3 \le |k| \le 10} k^{-3} \cos(\mathbf{k} \cdot \mathbf{x} + \phi_k), \tag{4.2}$$

$$v = -FX + \sum_{3 \le |k| \le 10} k^{-3} \cos(\mathbf{k} \cdot \mathbf{x} + \phi_k), \tag{4.3}$$

$$\rho = -Z + \sum_{3 \le |k| \le 10} k^{-3} \cos(\mathbf{k} \cdot \mathbf{x} + \phi_k), \tag{4.4}$$

where ϕ_k is the random phase shift in $[0, 2\pi]$. To investigate the effect of small scale perturbations to the system (2.27) with different rotation forces, we numerically simulate the system with the above initial data. We illustrate the development of perturbations with plots of perturbation energy and some snapshots of representative density, velocity field, generalized rotating enstrophy. We are also exam the motion of the perturbation dynamics.

4.1.1 No Stratification Limiting Dynamics

We first study the two dimensional Boussinesq system without stratification. The nondimensional system of (2.26) is simulated by pseudospectral method with 128 Fourier modes. In order to apply the exact solution theory from previous section, we fix the initial $\omega_0 = 1$, and vary the Rossby number to change the rotation force that is controlled by $F = Ro^{-1}$. Note that system (2.27) considered as no stratification since we removed the background density profile $\overline{\rho}$. The initial data is stably stratified. We study how the initial stable stratification reacts to the perturbations with rotation. Four different rotation regimes are tested, i.e., $Ro = 0.1, 1, 10$ strong rotation, intermediate rotation, and weak rotation, respectively. In our numerical test, we list all the numerical simulation parameters in the following table,

model parameter	
Ro	0.1 1 10
Domain	$[0, 2\pi] \times [0, 2\pi]$
Fourier mode	128×128
hyperviscosity ν_s	2e-15
hyperviscosity order Δ^s	s=8

Table 4.1: Model parameters that are used in the numerical experiments

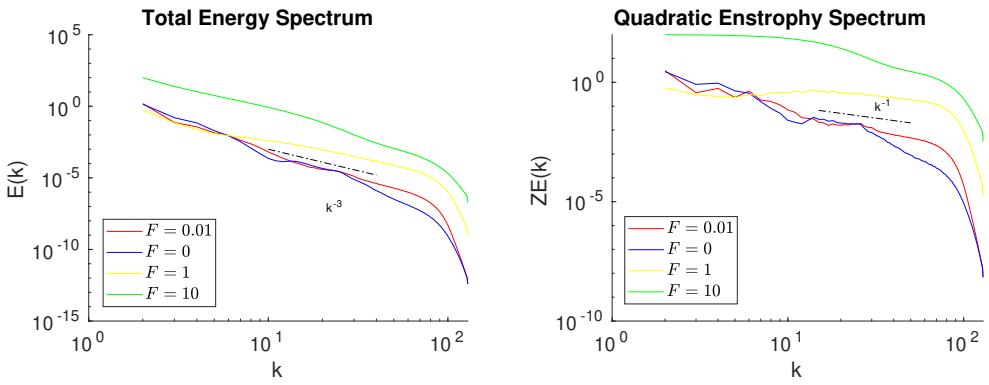

Figure 4.1: Radial averaged spectrum of total energy and generalized enstrophy

Energy transfer In the free-decay numerical cases, the total energy of the system (2.27) is conserved. When the rotation force weak, the potential energy $PE = \int \rho^2/2$ dominates in the system since the density is stably stratified $\rho = -z + \rho'$ at the beginning. As the system evolves, the density gradient $\nabla\rho$ changes resemble the Kelvin-Helmholtz instability due to small scale perturbations ρ'. The potential energy transfer into kinetic energy as the vorticity equation is driven by the density change. Small scales are generated and dissipated through hyper-viscosity. At equilibrium state, the flow field only includes

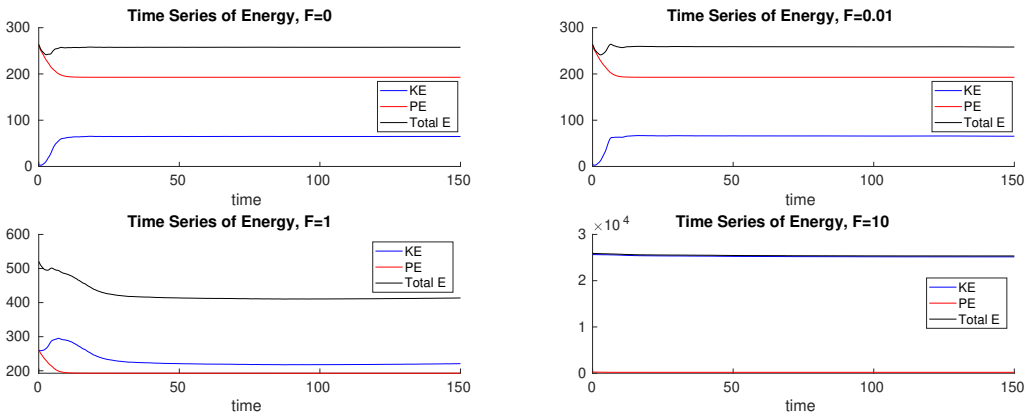

Figure 4.2: Time evolution of kinetic energy (blue line), potential energy (red line) and total energy (dark line)

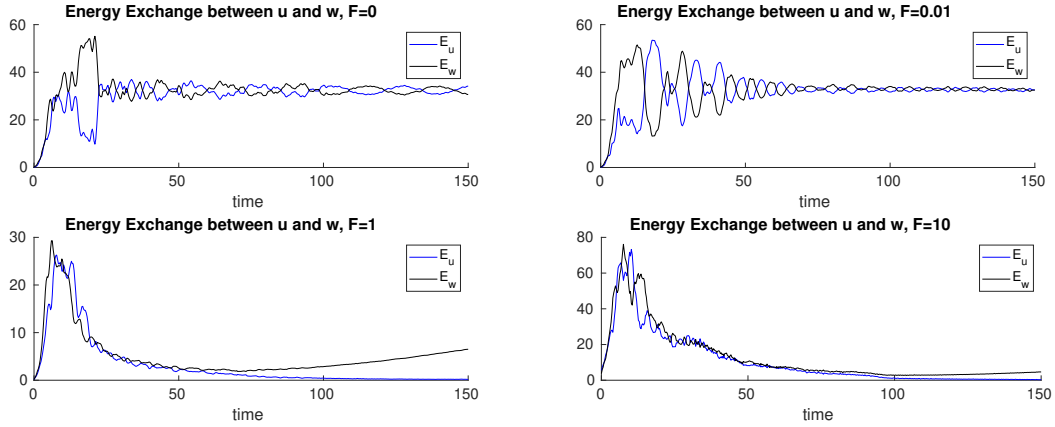

Figure 4.3:

large scale vortex which contain the most energy, $|\mathbf{k}| \leq 10$, see Fig. (4.1). The vortical flow with k^{-3} energy cascade is observed. When the rotation force becomes strong $Ro = 0.1, 1$, $Ro^{-1}v_z$ acts onto the vorticity equation yielding velocity field change. The effect of density gradient change is suppressed by the rotation forcing, i.e., $Ro^{-1}v_z > \rho_x$. We can state that under high rotation, the system is determined by the v momentum equation. In the transient time $t = 30$, the velocity field displays overturning due to rotation; see the last two columns in Fig. (4.22). Downscale and upscale the energy transfer is shown in the spectrum. The decay rate with high rotation is nearly k^{-3}. Eventually, the velocity field converges to a vertical stream and generates vertical jets.

We know that the v momentum is decomposed into $v = -Fx + v'$. From the equation, we can see that as F increases, the v is dominated by the background $-Fx$; consequently, the velocity v exhibits horizontal stratification. This can be verified from Fig. (**??**).

When $F = 0$, the small scale perturbation v' will be dissipated by hyperviscosity, and eventually decays to zero. There is no v momentum exchange since $Dv/Dt = 0$. In the no rotation case, the vorticity equation ω in (2.27) is driven by the density gradient ρ_x indicating the velocity field $(u, w)^T$ is also determined by the density. Fig. (4.22) shows velocity field contains large scale vortex resemble vortical flow for $F = 0$. The total energy is all contributed by velocity u and w. Energy exchange takes place only between u and w, see Fig. (4.3). As rotation effect starts, $F = 0.01$, $-Fu$ enters into the $v-$momentum equation and contribute to the total energy. The evolution of velocity v displays some large scale vortex structures due to rotation. When the effect of rotation becomes strong, $F = 1, 10$, the v velocity shows vertical jets. There is no pure energy exchange behavior among u and w, and the energy contribution of u and w decreases. Since the total energy is conserved, the contribution of v to the energy increases and dominates, see the bottom two plots in Fig. (4.22).

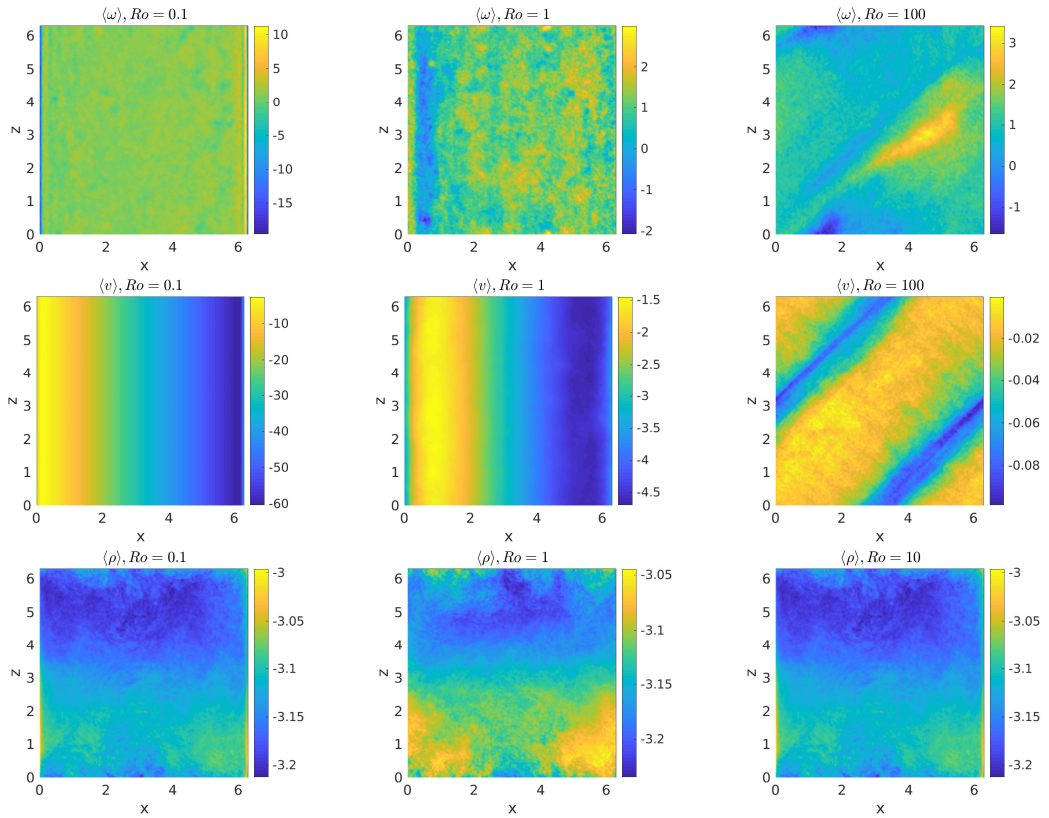

Figure 4.4: Mean field of ω, v, and ρ. From left to right, the rotation effects are $Ro = 0.1, 1, 10$.

statistical analysis

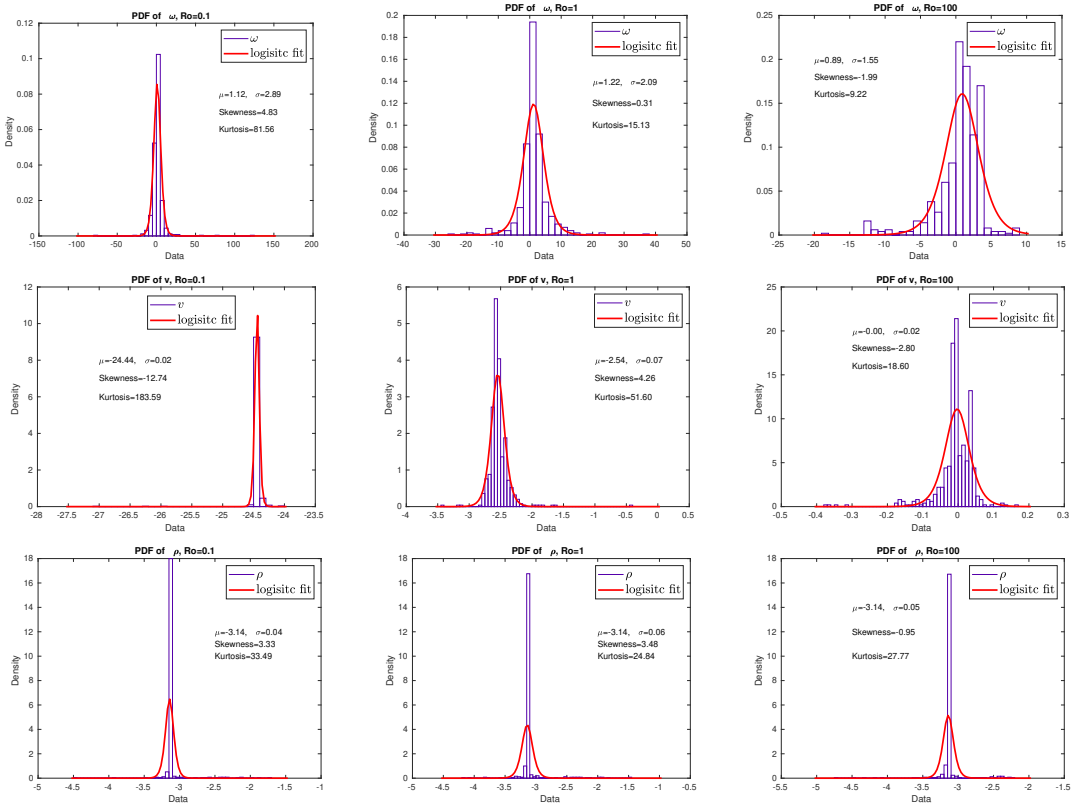

Figure 4.5: Probability density function of equilibrium states from ω, v, and ρ. From left to right, the rotation effects are $Ro = 0.1, 1, 10$.

mode interaction From Fig. (4.6), we can see that the correlation time of wave mode is shorter than the vortical mode. This is consistent with theory since we know that the PV component acts as large scale slow dynamics whereas the wave components are fast dynamics.

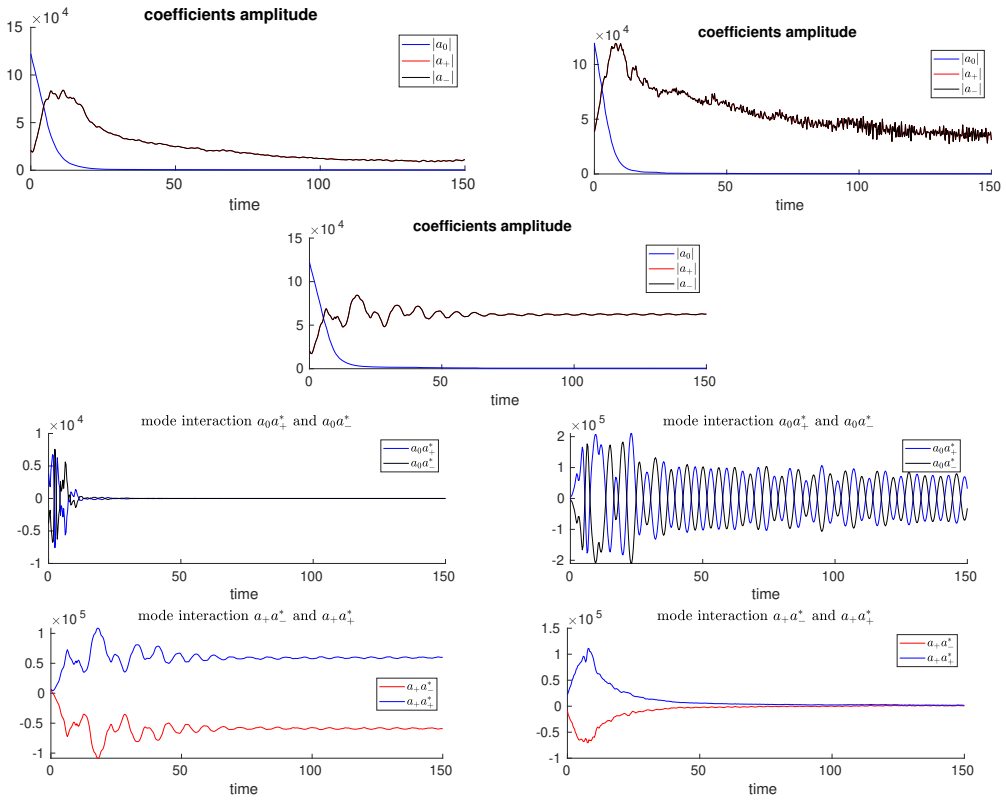

Figure 4.6: Top row is coefficients amplitude $|a_\alpha|$,

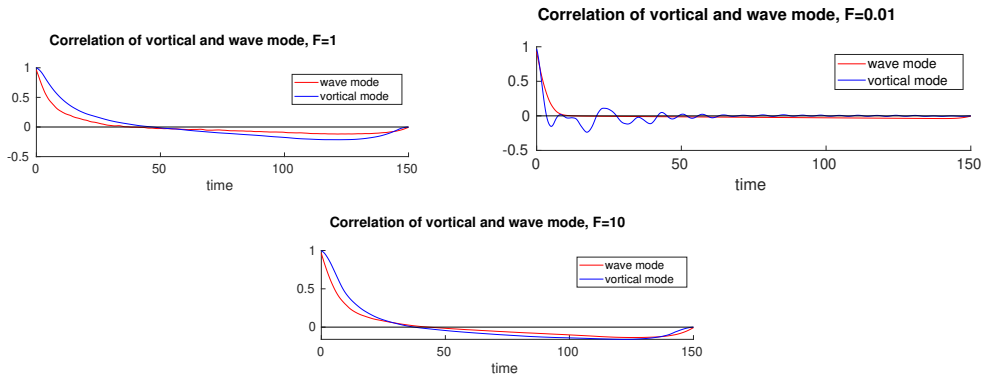

Figure 4.7: Autocorrelation of the vortical and wave mode coefficients of (2.27) under $F = 0.1, 1, 10$.

With no background stratification, the density equation is $D\rho/Dt = 0$. The small scale perturbation to the initial stably stratified flow causes instability and changes the flow completely. The perturbation ρ' at height z is equivalent to transporting fluid along the density gradient from either above or below depending on the sign of ρ'

$$\rho(z+h) = -z + \rho' \approx -z + h\frac{d(-z)}{dz} \tag{4.5}$$

From the above Taylor expansion, we find the perturbation $\rho' \approx -h$. The potential energy change due to gravity work is,

$$\int g\rho' dz = -gh^2/2. \tag{4.6}$$

For initially stable stratified flow, it is obvious to see that the potential energy will drop due to the gravity work for the perturbation. At the beginning transient regime, the density field exhibits Kelvin-Helmhotlz instability, see (**??**). The potential energy transferred into kinetic energy, whereas the total energy is conserved, see (4.2). After saturation, the small scales are dissipated, and the density field only contains large scales. The effect of rotation turns the density to vertical motion. Finally, we look at the evolution of enstrophy. We can expect the strength of the vorticity field is reduced under weak rotation. Therefore, based only in the scalar value, we can conclude that the generalized enstrophy (2.16) decay in time. The enstrophy spectrum tells that the small scales ($|\mathbf{k}| \leq 80$) are generated as the vorticity intensity is increased when rotation is considered.

Perturbation Motion Previously, we studied at the evolution of the whole system (2.27), starting with stable stratification. Here, we only look at the dynamics of perturbation and numerically to investigate the perturbation motion. If we decompose the flow field into,

$$\omega = \omega(x,z) + \omega(x,z,t)', \vec{u} = \vec{V}(x,z) + \vec{u}', \rho = \overline{\rho}(x,z,) + \rho(x,z,t)', \tag{4.7}$$

the perturbation dynamics of system (2.27) can be simplified into the following

$$\begin{aligned} \omega'_t + \nabla^\perp\psi' \cdot \nabla\omega' + \vec{V} \cdot \nabla\omega' &= Fv'_z + \rho'_x, \\ v'_t + \nabla^\perp\psi' \cdot \nabla v' + \vec{V} \cdot \nabla v' &= 0, \\ \rho'_t + \nabla^\perp\psi' \cdot \nabla\rho' + \vec{V} \cdot \nabla\rho' &= w', \\ \omega' &= -\Delta\psi', \end{aligned} \tag{4.8}$$

with $\vec{u}' = (u', w')^T = \nabla^\perp\psi' = (-\psi'_z, \psi'_x)$, and $\vec{V} = (V_1, V_3)^T$ are given by the shear flow exact solution (4.2). It is obvious to see that the rotation f does not affect the perturbation v' momentum equation. The Richardson number is fixed $Ri = 1$ following the previous scale. We run the system (4.8) with random initial condition at $F = 0, 0.01, 1, 10$. The four different rotation dynamical regimes are the same as in the previous section. The numerical results reveal that no significant amplification in the perturbation amplitudes under weak rotation condition. However the amplitudes increase for strong rotation

$F = 1, 10$. The evolution of perturbations is illustrated by the characteristic density, velocity field, and energy spectrum. A general picture of perturbation evolution is given by the plots of velocity and density in Fig. (4.8) and (4.9). To illustrate how perturbations undergo transient growth, we selected two different moments of time, $t = 30, 150$ to present the motion. When there is no rotation ($F = 0$) or rotation is weak ($F = 0.01$), perturbations are mainly confined to small scales $t = 30$ and produce overturning, see Fig. (4.8), (4.9). The perturbations are stable without the growth of amplitude. In these dynamical regime, the perturbation energy shows inverse cascade with nearly ratio $k^{-5/3}$ and the small scale vortex are dominate as the largest enstrophy are among high wave numbers ($30 \leq |\mathbf{k}| \leq 60$), see (4.10). When rotation force becomes $F = 1, 10$, large scale vortex are generated. Perturbations are largely confined to the large scales, which are a signature of Kelvin-Helmhotlz instability, see Fig. (4.9). The energy decay with nearly k^{-3} and the intensity of large scale vortex is increased as the enstrophy spectrum contributes most when $|\mathbf{k}| \leq 10$, which is completely different than the weak rotation dynamical regime. As a final comment, we mention that these results show that linear shear flows are stable to perturbations under weak rotation. When rotation force becomes strong, however, it is unstable as the perturbation amplitudes grow. The effect of rotation changes the dynamical of perturbations.

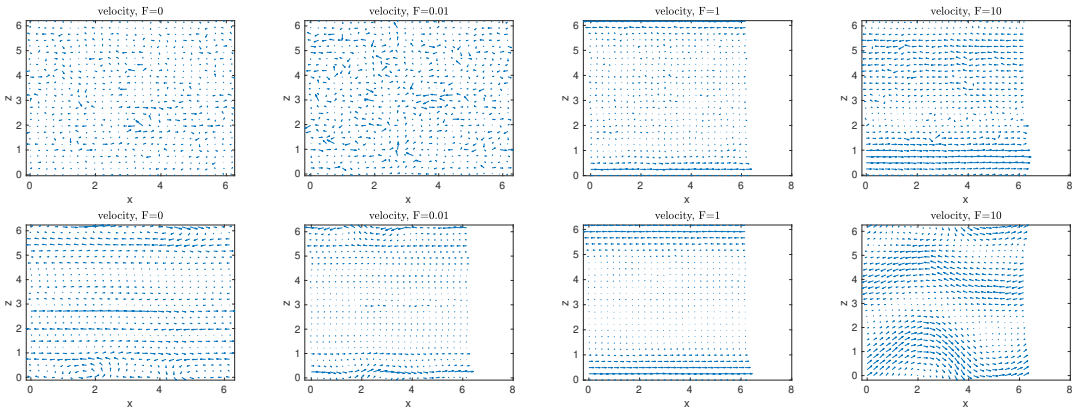

Figure 4.8: Perturbation velocity field $(u, w)^T$ snapshots at $t = 30$ (top row) and $t = 150$ (bottom row). From left to right, the rotation effects are $F = 0, 0.01, 1, 10$.

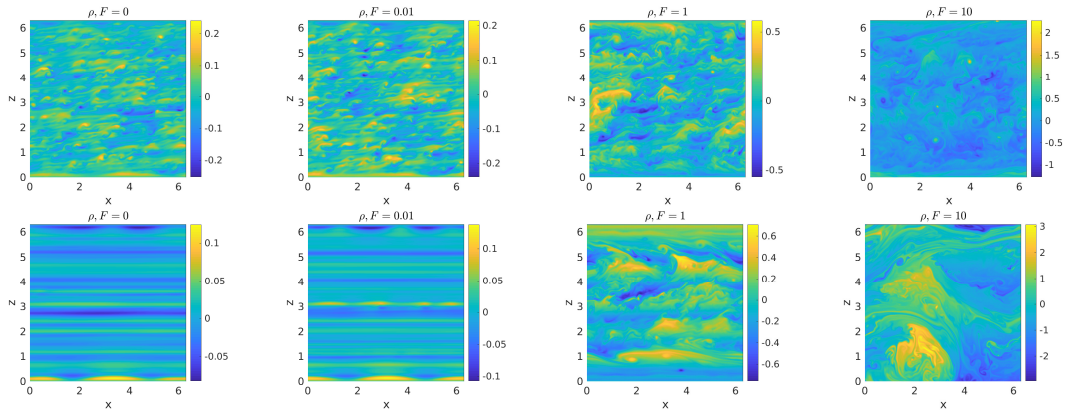

Figure 4.9: Perturbation density ρ snapshots at $t = 30$ (top row) and $t = 150$ (bottom row). From left to right, the rotation effects are $F = 0, 0.01, 1, 10$.

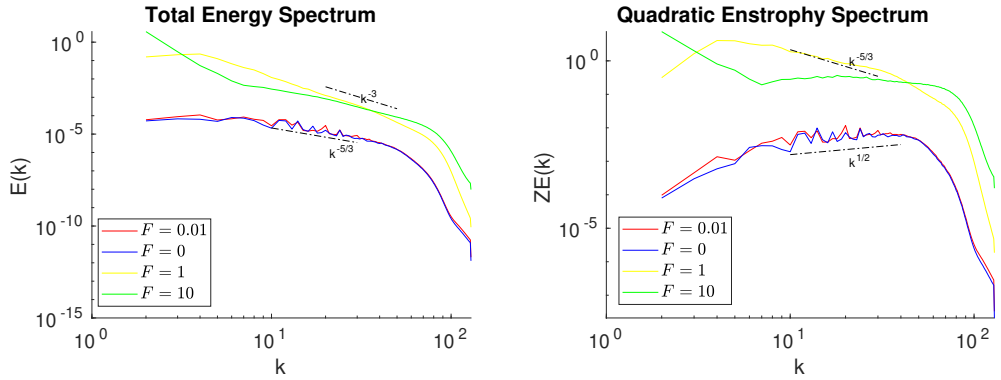

Figure 4.10: Perturbation energy spectrum (left) and generalized enstrophy spectrum (right)

4.1.2 No Rotation limiting dynamics

In the previous section, we have replaced the background density $\overline{\rho}$ by the exact solution of shear flow $\rho = \rho_b + \vec{b} \cdot \mathbf{x}$ in our numerical studies. We have seen that there is no stratification in the limiting dynamical regime with different rotation forces. The rotation force plays an important role in the velocity field change resulting in a horizontal stratification. In this section, we enforce a background density profile for the exact solution,

$$\rho = \rho_b + \overline{\rho} + \rho \cdot \mathbf{x}. \tag{4.9}$$

The vorticity and v momentum equations are stay the same, but the density equation turns into,

$$\rho_t + \nabla^{\perp}\psi \cdot \nabla\rho = Fr^{-1}w. \tag{4.10}$$

In our numerical tests, we list the following parameters that are used.

model parameter	
Fr	0.1 1 10
Domain	$[0, 2\pi] \times [0, 2\pi]$
Fourier mode	128×128
hyperviscosity ν_s	2e-15
hyperviscosity order Δ^s	s=8

Table 4.2: Model parameters that are used in the numerical experiments

By enforcing a background density, we introduce gravity wave in the system. The evolution of the system is shown in Fig. (4.11) with velocity and density at two moments, $t = 30$ and $t = 150$. We run the system with three Froud number regime. The initial small scale perturbations cause instability in the transient regime. It can be seen from the Fig. (4.11) that the density exhibits stratification with overturning. However, the

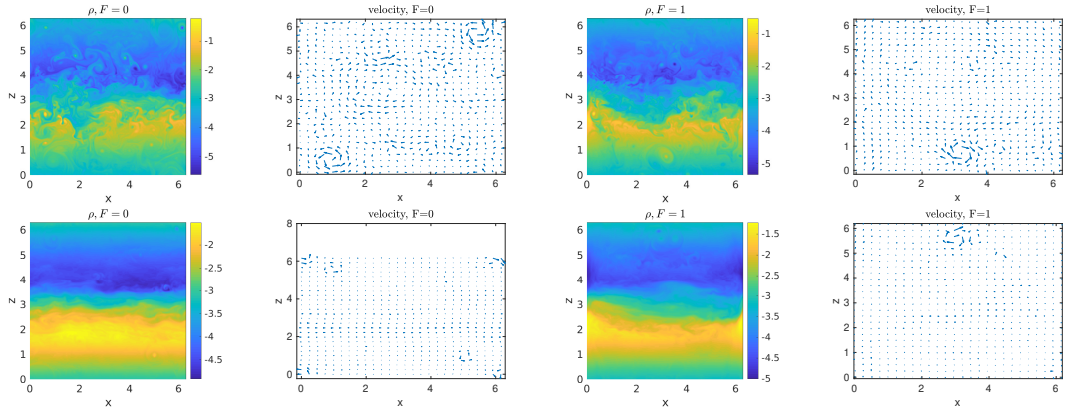

Figure 4.11: density ρ and velocity field (u, w) snapshots of system (4.10) at $t = 30$ (top row) and $t = 150$ (bottom row). The left two columns are results without rotation $F = 0$, the right two columns are generated under $F = 1$.

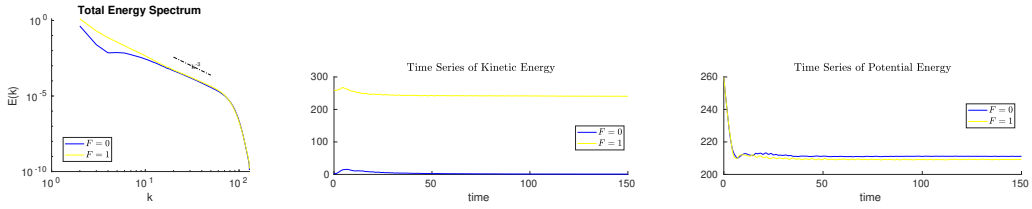

Figure 4.12: Total energy spectrum of the system (4.10) with stratification (left), and evolution of kinetic (middle) and potential energy (right)

rotation is the major effect for v momentum since $Dv/Dt = -Fu$. The v compoenent displays horizontal stratification when rotation is strong. For the two cases studied here, they shown similar energy spectrum with decay rate k^{-3} and a clearly downscale energy

transfer, see Fig. (4.12). At early time, the potential energy decays due to gravity work for small scale perturbations and transferred into kinetic energy. Therefore, the kinetic energy increases at the beginning. At later time, because of generation of small scale structures dissipation is not negligible, so the kinetic energy decreases but the total energy is conserved.
The main difference between the system (4.10) and (2.27) is that we enforce a background stratification at (4.10) which introduces gravity wave. In the system (2.27), the density is completely changed and exhibits large scale vertical flow at equilibrium even it is stable stratified initially. This is caused by the initial small scale perturbations. In the system (4.10), however, the density shown stable stratification at steady state. The effect of small scale perturbation is alleviated by the restoring frequency from gravity wave.

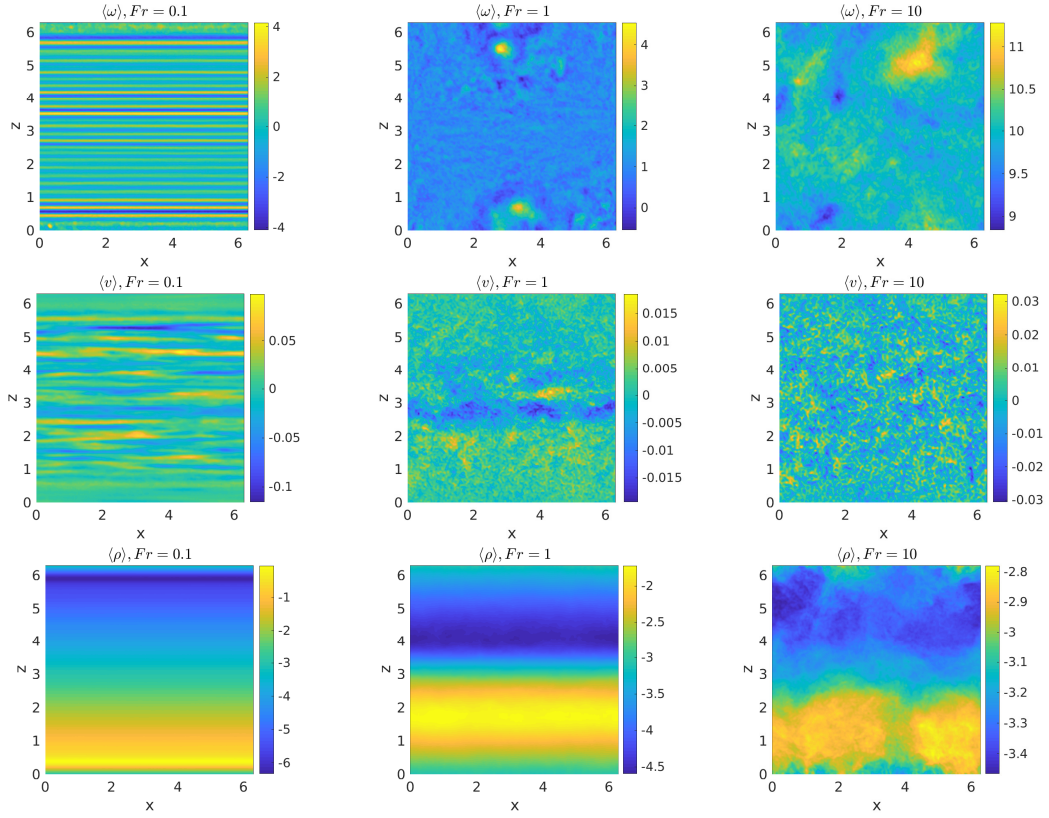

Figure 4.13: Mean field of ω, v, and ρ. From left to right, the stratification effects are $Fr = 0.1, 1, 10$.

statistical analysis

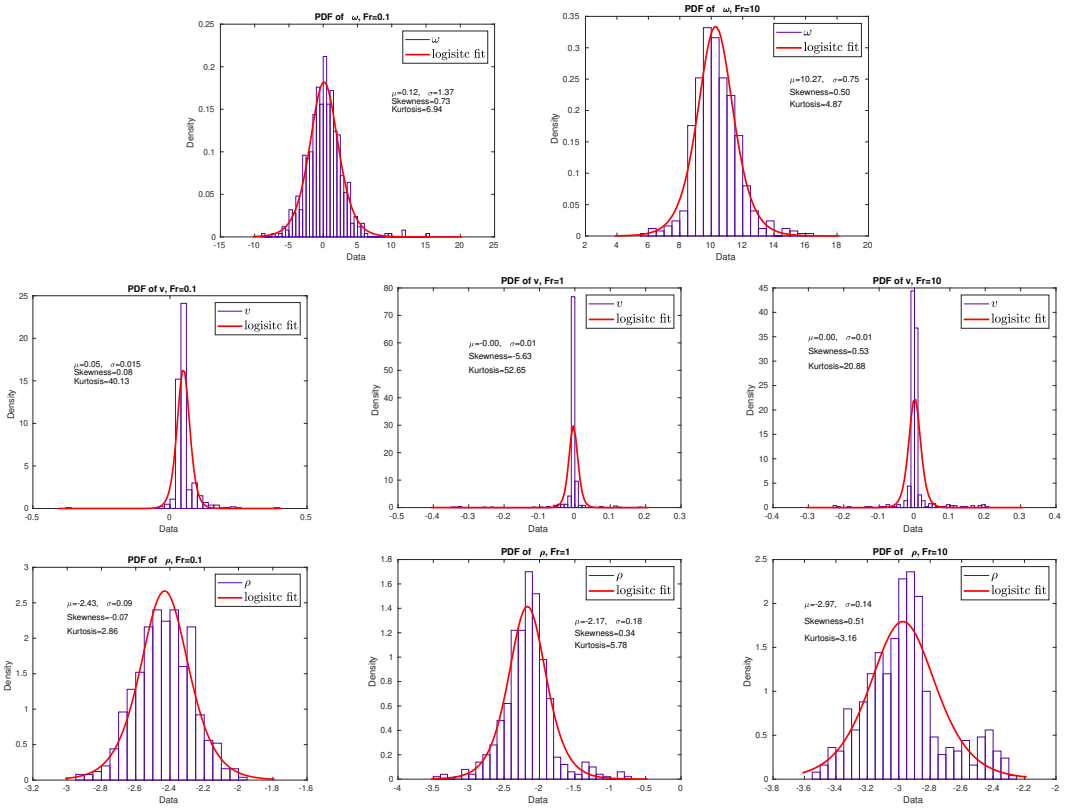

Figure 4.14: Probability density function of equilibrium states from ω, v, and ρ. From left to right, the stratification effects are $Fr = 0.1, 1, 10$.

4.2 Forced-dissipative Numerical Simulation

4.2.1 No Stratification

In the previous section, we thoroughly discussed the two dimensional Boussinesq system (2.27) with shear flow exact solution under different rotation forces. We did not consider the external forcing and dissipation in the system. In this section, we study the small scale random forcing for system (4.15). After add damping and forcing, the equations become

$$\begin{aligned} \omega_t + \nabla^\perp\psi\cdot\nabla\omega &= Ro^{-1}v_z + \rho_x + \quad \mu\Delta\omega + \mu_s\Delta^s\omega + \boldsymbol{F}_\omega, \\ v_t + \nabla^\perp\psi\cdot\nabla v &= -Ro^{-1}u + \qquad \mu\Delta + \mu_s\Delta^s v + \boldsymbol{F}_v, \\ \rho_t + \nabla^\perp\psi\cdot\nabla\rho &= \qquad\qquad \mu\Delta\rho + \mu_s\Delta^s\rho + \boldsymbol{F}_\rho, \\ \omega &= -\Delta\psi. \end{aligned} \tag{4.11}$$

The initial conditions are the same shear flow solutions and small scale random perturbation,

$$\begin{aligned} \omega(t=0) &= \omega_0 + \sum_{3\le k\le 10} k^{-3}\exp(i(\mathbf{k}\cdot x+\phi_k)) + c.c. \\ \theta(t=0) &= \theta_0 + \sum_{3\le k\le 10} k^{-3}\exp(i(\mathbf{k}\cdot x+\phi_k)) + c.c., \\ v(t=0) &= v_0 + \sum_{3\le k\le 10} k^{-3}\exp(i(\mathbf{k}\cdot x+\phi_k)) + c.c., \end{aligned} \tag{4.12}$$

where θ_0, ω_0, v_0 are the shear flow exact solutions in (2.20). We consider different cases with Ro. The vertical and horizontal ratio $H/L = 1$ (H and L are the vertical and horizontal length). The double periodic condition is used in the numerical simulation. The stochastic forcing is decomposed into each mode,

$$\boldsymbol{F}(\mathbf{x},t) = \sigma(\mathbf{x})\dot{W}_t = \sum_{\mathbf{k}} \sigma_k \dot{W}_{k,t} e^{i\mathbf{k}\cdot\mathbf{x}}, \tag{4.13}$$

where $\dot{W}_k$ is independent with different wavenumbers. The correlations in $\boldsymbol{F}$ imply the spectral coefficient is determined by the Fourier transform of the correlation, $|\sigma_k|^2 = \Sigma_k$. We add the random forcing on a small scale k_f with energy injection rate ϵ_f,

$$\Sigma_k = \epsilon_f \frac{exp(-\frac{(k-k_f)^2}{2\sigma^2})}{\sqrt{2\pi}\sigma}. \tag{4.14}$$

In our numerical test, we choose $k_f = 24$, $\epsilon_f = 0.01$. We list all the numerical simulation parameters in the following table,

Energy transfer The time evolution of kinetic energy and potential energy is shown in 4.15. For initial stable stratified flow, the potential energy decays at the early time due to gravity work to the perturbations and the dissipation of density. For different rotation

model parameter	
Ro	0.1 1 10
k_f	24
Domain	$[0, 2\pi] \times [0, 2\pi]$
Energy injection ϵ_f	0.01
Fourier mode	128×128
hyperviscosity ν_s	2e-15
hyperviscosity order Δ^s	s=8
Reynolds number scale Re	5000
Prandtl number Pr	1

Table 4.3: Model parameters that are used in the numerical experiments

regime, the kinetic energy did not increase as time evolve. After a short period of initial growth, the kinetic energy does not grow in time and reaches statistical equilibrium after $t = 60$. The enstrophy increases intermittently. There is a non-normal transient growth of enstrophy for strong rotation $Ro = 0.1$. We can expect the strength of the vortex is strong due to high rotation during this time. After around $T = 80$, the enstrophy decreases and reduce to similar amplitude as other rotation force regime, see see (4.16). From the energy spectrum, we can see that downscale energy cascade with a rate nearly k^{-2}. All of the energy input by the random force is dissipated at small scales by viscosity. Energy is transferred simultaneously to large and small scales.

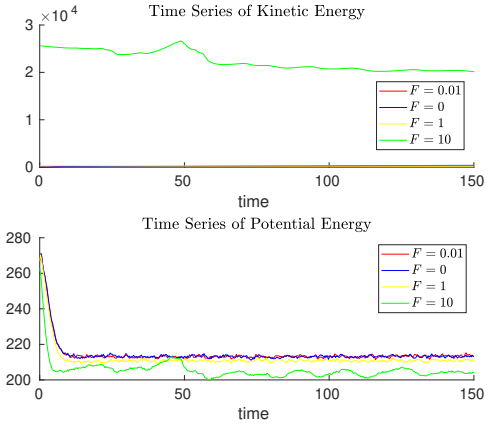

Figure 4.15: Radial averaged spectrum of total energy and generalized enstrophy

When rotation is weak, the velocity exhibits large scale vortical flow, see Fig. (4.17). For high rotation, however, the velocity field is confined to vertical flow. This is similar to the non-dissipative and non-forcing case in the previous section. From the previous results, we know that the v momentum has horizontal stratification for high rotation. Due to small scale random forcing, however, the horizontal stratification of v momentum is destroyed, see (4.18). This is because the vertical motion of small scales resembles the

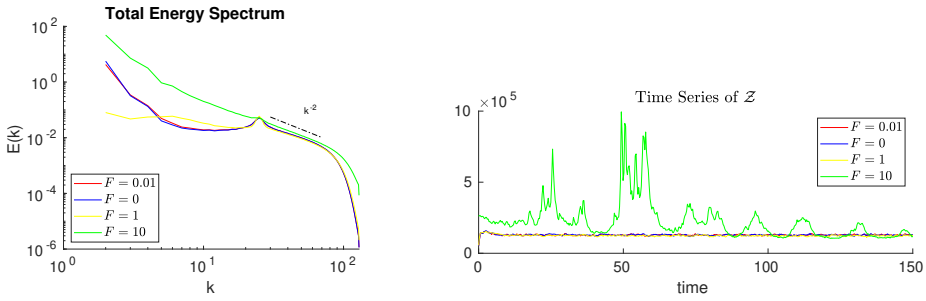

Figure 4.16: Radial averaged spectrum of total energy and generalized enstrophy

Kelvin-Helmotlz (KH) instability, which turns the v momentum field into the columnar flow. They show similar evolution as the small scale motion is driven by the large scale,

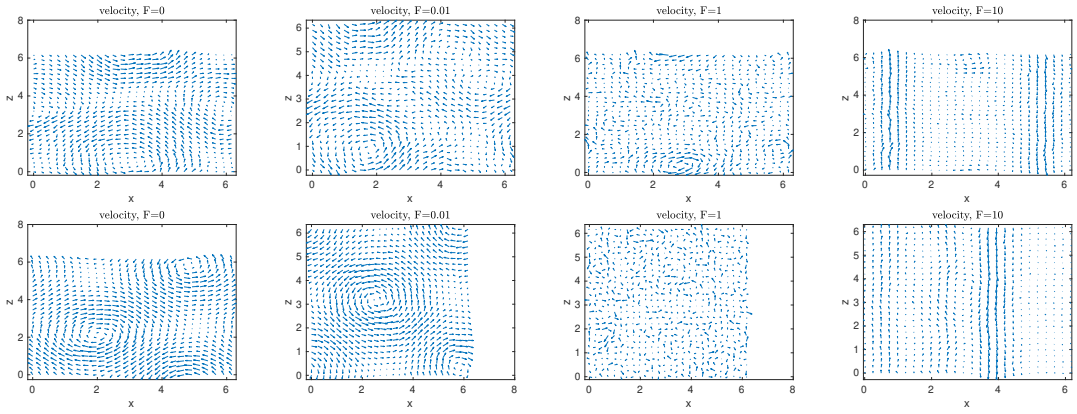

Figure 4.17: Velocity field $(u, w)^T$ snapshots at $t = 30$ (top row) and $t = 150$ (bottom row). From left to right, the rotation effects are $F = 0, 0.01, 1, 10$. Forcing scale is $k_f = 24$, energy injection rate $\epsilon = 0.01$

see Fig. (4.18). The density displays a similar columnar flow.

statistical analysis The mean field and probability density function associated with the turbulent states are plotted.

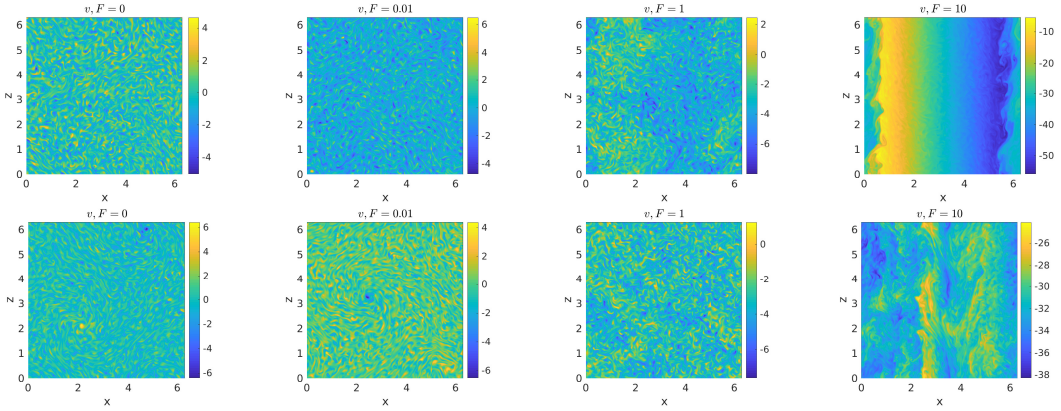

Figure 4.18: Velocity v component snapshots at $t = 30$ (top row) and $t = 150$ (bottom row). From left to right, the rotation effects are $Ro =, 0.1, 1, 10$.

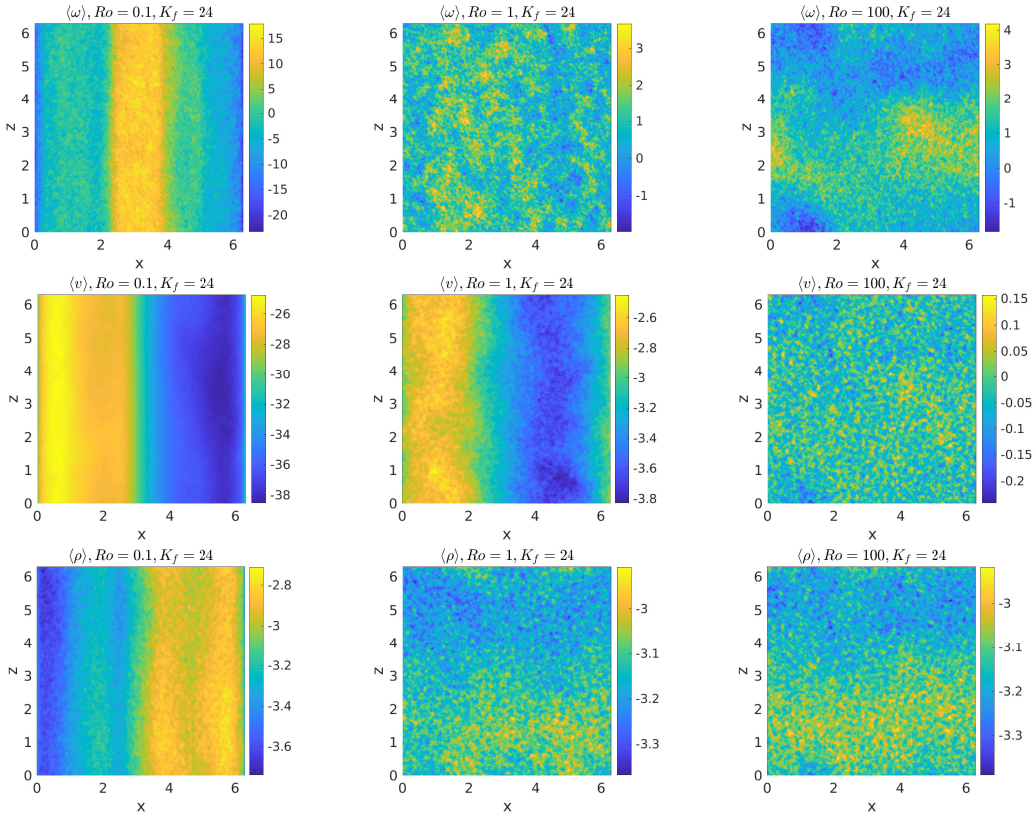

Figure 4.19: Mean field of ω, v, and ρ. From left to right, the stratification effects are $Ro = 0.1, 1, 10$.

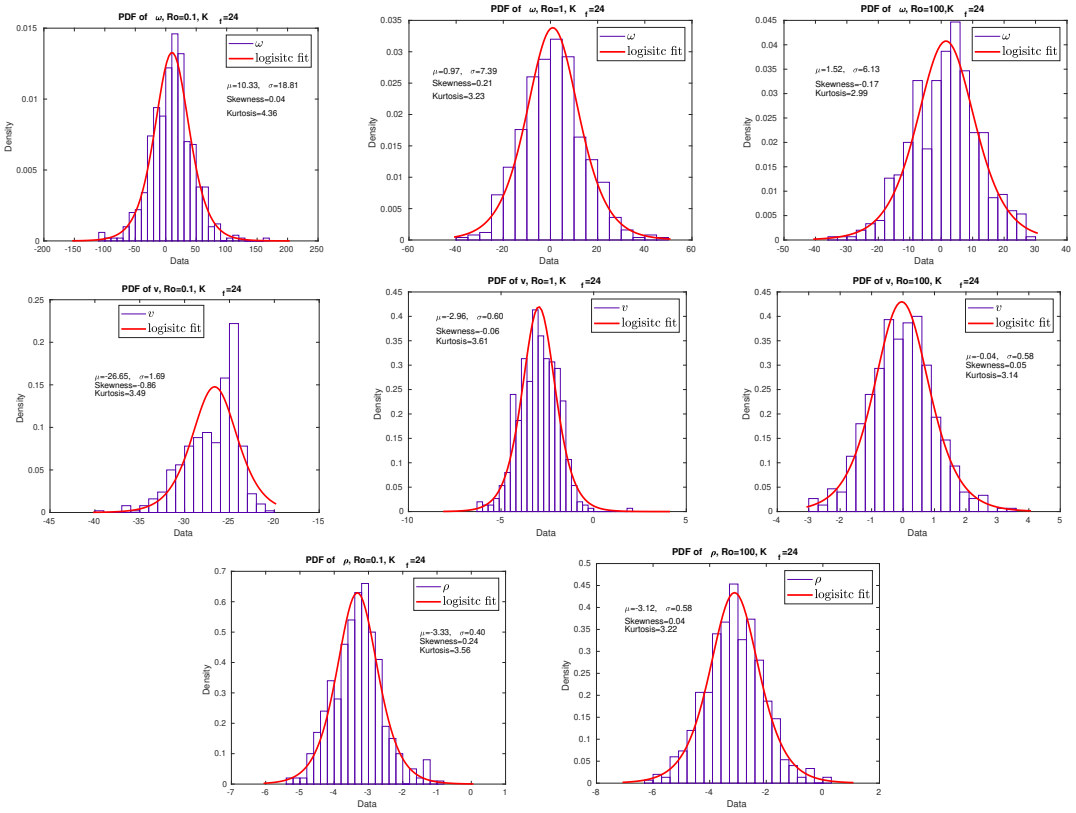

Figure 4.20: Probability density function of equilibrium states from ω, v, and ρ. From left to right, the stratification effects are $Ro = 0.1, 1, 10$.

4.2.2 No Rotation

In this section, we study the small scale random forcing for the stably stratified system (4.15) without rotation. After add damping and forcing, the equations become

$$\begin{aligned} \omega_t + \nabla^\perp\psi\cdot\nabla\omega &= Fr^{-1}\rho_x + \quad \mu\Delta\omega + \mu_s\Delta^s\omega + \boldsymbol{F}_\omega, \\ v_t + \nabla^\perp\psi\cdot\nabla v &= \qquad\qquad \mu\Delta + \mu_s\Delta^s v + \boldsymbol{F}_v, \\ \rho_t + \nabla^\perp\psi\cdot\nabla\rho &= Fr^{-1}w + \quad \mu\Delta\rho + \mu_s\Delta^s\rho + \boldsymbol{F}_\rho, \\ \omega &= -\Delta\psi. \end{aligned} \tag{4.15}$$

We test the system with different Froud number. The initial conditions are the same as the previous section. The following parameters are used,

model parameter	
Fr	0.1 1 10
k_f	24
Domain	$[0, 2\pi] \times [0, 2\pi]$
Energy injection ϵ_f	0.01
Fourier mode	128×128
hyperviscosity ν_s	2e-15
hyperviscosity order Δ^s	s=8
Reynolds number scale Re	5000
Prandtl number Pr	1

Table 4.4: Model parameters that are used in the numerical experiments

conclusion and future work

In this report, we studied the two dimensional Boussinesq system with rotation and stratification. We numerically investigate the effect of small scale perturbations to the shear flow exact solution. In the free-decay case, the small scale perturbations change the density motion under different rotation forces with no background stratification behavior. At steady state, all density fields are confined to large scale motion since all small scales are dissipated through hyper viscosity. The strong rotation force turns the flow into columnar flow resulting in a horizontal stratification for v momentum. After we add strong random forcing onto the system, small scales are dominant in the transient regime. At the equilibrium stage, the small scales motion is driven by large scale. Similarly, the flow field becomes vertical flow under high rotation force. When we enforce a background density ($\overline{\rho}$) in the free-decay case, the density exhibits stable stratification. As time evolve, small scale oscillations will be observed. The nature restoring frequency of the stably stratified fluid acts faster than the destabilizing effect, which causes the system remain stable stratified. The total energy and enstrophy spectrum is shown in Fig. **??**. The energy decay rate $k^{-5/3}$ can be observed and matches the same quantity in the reference [5, 20]. The total energy is conserved without damping and forcing, see Fig. **??**.

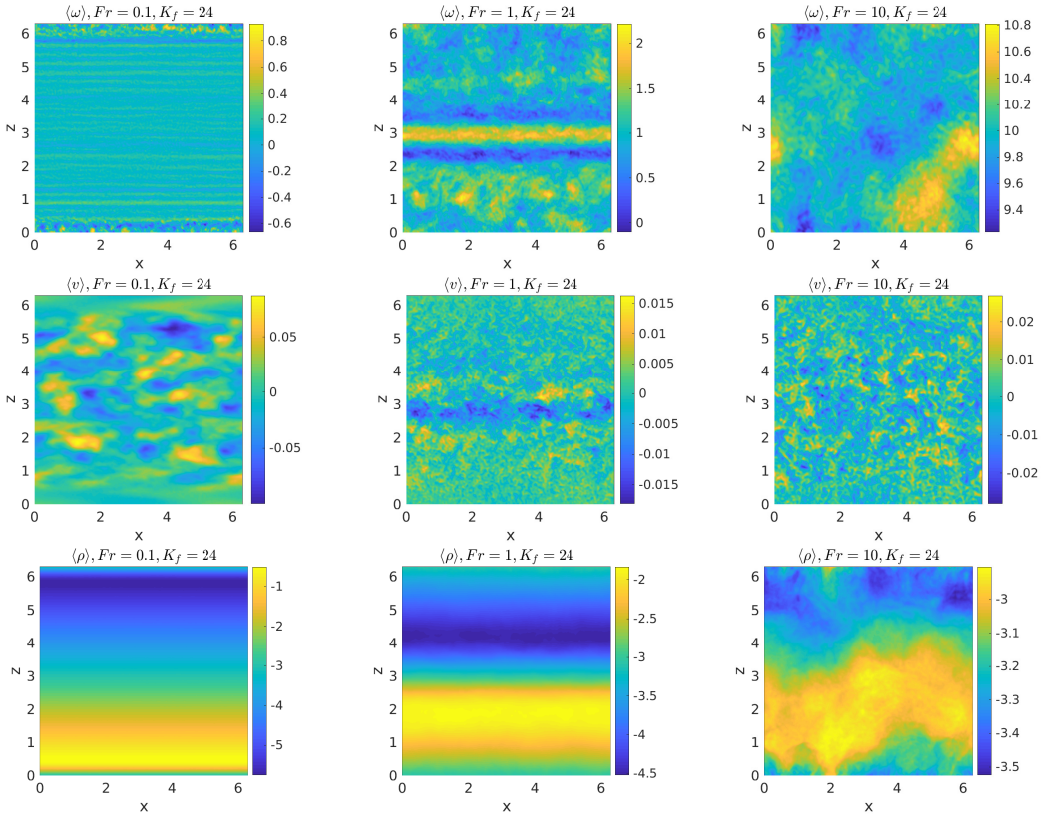

Figure 4.21: Mean field of ω, v, and ρ. From left to right, the stratification effects are $Fr = 0.1, 1, 10$.

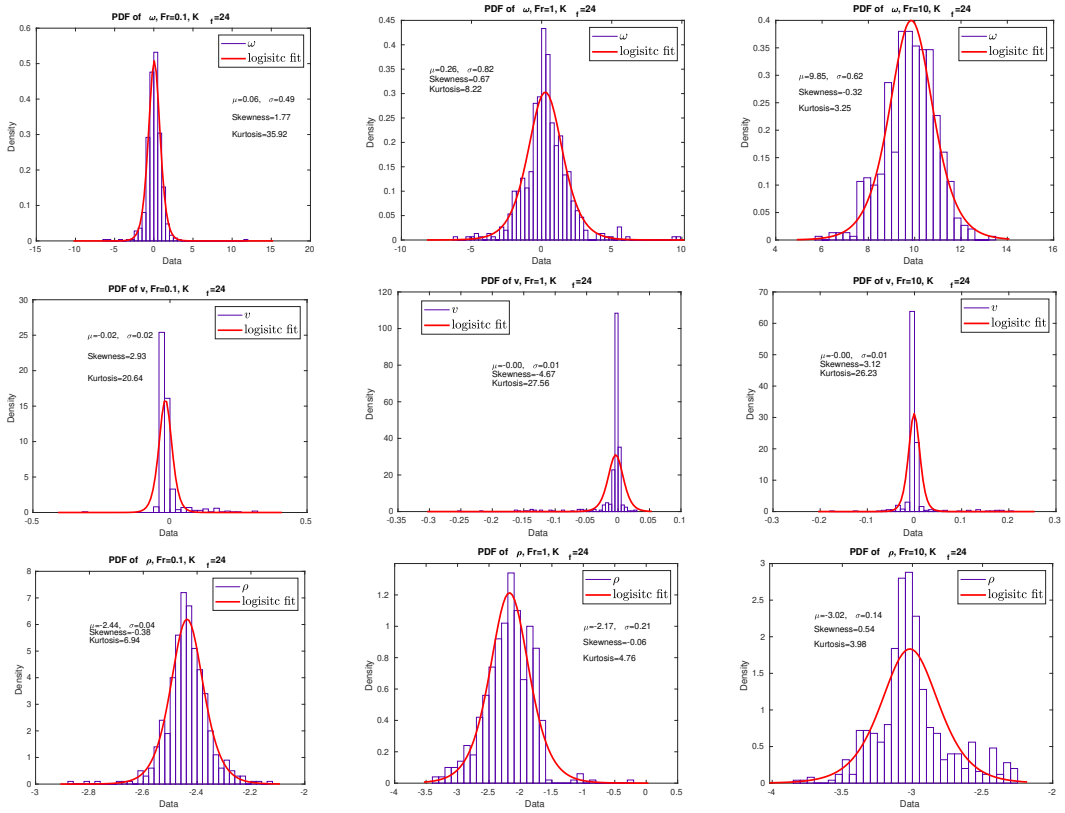

Figure 4.22: Probability density function of equilibrium states from ω, v, and ρ. From left to right, the stratification effects are $Fr = 0.1, 1, 10$.

References

[1] Peter Bartello. Geostrophic adjustment and inverse cascades in rotating stratified turbulence. *Journal of the atmospheric sciences*, 52(24):4410–4428, 1995.

[2] Nan Chen and Andrew J Majda. Filtering nonlinear turbulent dynamical systems through conditional gaussian statistics. *Monthly Weather Review*, 144(12):4885–4917, 2016.

[3] Pedro F Embid. Averaging over fast gravity waves for geophysical flows with arbitary. *Communications in Partial Differential Equations*, 21(3-4):619–658, 1996.

[4] Pedro F Embid and Andrew J Majda. Low froude number limiting dynamics for stably stratified flow with small or finite rossby numbers. *Geophysical & Astrophysical Fluid Dynamics*, 87(1-2):1–50, 1998.

[5] Gerardo Hernandez-Duenas, Leslie M Smith, and Samuel N Stechmann. Investigation of boussinesq dynamics using intermediate models based on wave–vortical interactions. *Journal of Fluid Mechanics*, 747:247–287, 2014.

[6] Andrew Majda. *Introduction to PDEs and Waves for the Atmosphere and Ocean*, volume 9. American Mathematical Soc., 2003.

[7] Andrew Majda and Nan Chen. Model error, information barriers, state estimation and prediction in complex multiscale systems. *Entropy*, 20(9):644, 2018.

[8] Andrew J Majda and Pedro Embid. Averaging over fast gravity waves for geophysical flows with unbalanced initial data. *Theoretical and computational fluid dynamics*, 11(3-4):155–169, 1998.

[9] Andrew J Majda and Marcus J Grote. Model dynamics and vertical collapse in decaying strongly stratified flows. *Physics of fluids*, 9(10):2932–2940, 1997.

[10] Andrew J Majda and Di Qi. Strategies for reduced-order models for predicting the statistical responses and uncertainty quantification in complex turbulent dynamical systems. *SIAM Review*, 60(3):491–549, 2018.

[11] Andrew J Majda and Michael G Shefter. Elementary stratified flows with instability at large richardson number. *Journal of Fluid Mechanics*, 376:319–350, 1998.

[12] Andrew J Majda and Michael G Shefter. Nonlinear instability of elementary stratified flows at large richardson number. *Chaos: An Interdisciplinary Journal of Nonlinear Science*, 10(1):3–27, 2000.

[13] C Henry McComas and Francis P Bretherton. Resonant interaction of oceanic internal waves. *Journal of Geophysical Research*, 82(9):1397–1412, 1977.

[14] AD McEwan. Degeneration of resonantly-excited standing internal gravity waves. *Journal of Fluid Mechanics*, 50(3):431–448, 1971.

[15] AD McEwan, DW Mander, and RK Smith. Forced resonant second-order interaction between damped internal waves. *Journal of Fluid Mechanics*, 55(4):589–608, 1972.

[16] John W Miles. On the stability of heterogeneous shear flows. *Journal of Fluid Mechanics*, 10(4):496–508, 1961.

[17] Peter Müller, Greg Holloway, Frank Henyey, and Neil Pomphrey. Nonlinear interactions among internal gravity waves. *Reviews of Geophysics*, 24(3):493–536, 1986.

[18] OM Phillips. On the dynamics of unsteady gravity waves of finite amplitude part 1. the elementary interactions. *Journal of Fluid Mechanics*, 9(2):193–217, 1960.

[19] OM Phillips. Wave interactions-the evolution of an idea. *Journal of Fluid Mechanics*, 106:215–227, 1981.

[20] Mark Remmel, Jai Sukhatme, and Leslie M Smith. Nonlinear inertia-gravity wave-mode interactions in three dimensional rotating stratified flows. *arXiv preprint arXiv:0903.0693*, 2009.

[21] James J Riley and Marie-Pascale Lelong. Fluid motions in the presence of strong stable stratification. *Annual review of fluid mechanics*, 32(1):613–657, 2000.

[22] Chantal Staquet and Joël Sommeria. Internal gravity waves: from instabilities to turbulence. *Annual Review of Fluid Mechanics*, 34(1):559–593, 2002.